Neuronal vulnerability and multilineage diversity in multiple sclerosis

Lucas Schirmer[1,2,3,4*], Dmitry Velmeshev[1,5*], Staffan Holmqvist[2], Max Kaufmann[6], Sebastian Werneburg[7], Diane Jung[1,5], Stephanie Vistnes[1,4], John H. Stockley[2], Adam Young[8], Maike Steindel[2,8], Brian Tung[1,5,,9], Nitasha Goyal[1,5,,9], Aparna Bhaduri[1,5], Simone Mayer[1,5], Jan Broder Engler[6], Omer A. Bayraktar[2], Robin J. M. Franklin[8], Maximilian Haeussler[10], Richard Reynolds[11], Dorothy P. Schafer[7], Manuel A. Friese[6], Lawrence R. Shiow[1,4], Arnold R. Kriegstein[1,5†] and David H. Rowitch[1,2,4†]

[1]Eli and Edythe Broad Center of Regeneration Medicine and Stem Cell Research, University of California, San Francisco, San Francisco, CA 94143, USA; [2]Department of Paediatrics and Wellcome Trust-MRC Cambridge Stem Cell Institute, University of Cambridge, Cambridge, CB2 0QQ, UK; [3]Department of Neurology, Medical Faculty Mannheim, University of Heidelberg, 68167 Mannheim, Germany; Departments of [4]Pediatrics and [5]Neurology, University of California, San Francisco, San Francisco, CA 94158, USA; [6]Institute of Neuroimmunology and Multiple Sclerosis, Center for Molecular Neurobiology Hamburg, University Medical Center Hamburg-Eppendorf, 20251 Hamburg, Germany; [7]Department of Neurobiology and the Brudnik Neuropsychiatric Institute, University of Massachusetts Medical School, Worcester, MA 01605, USA; Departments of [8]Clinical Neurosciences and Wellcome Trust-MRC Cambridge Stem Cell Institute, University of Cambridge, Cambridge, CB2 0QQ, UK; [9]Department of Molecular and Cell Biology, University of California, Berkeley, CA, 94720; [10]Genomics Institute, University of California, Santa Cruz, CA, 95064, USA; [11]Division of Brain Sciences, Department of Medicine, Imperial College London, London W12 0NN, UK.

*These authors contributed equally

†Corresponding author

Abstract

Multiple sclerosis (MS) is a neuroinflammatory disease with a relapsing-remitting disease course at early stages, distinct lesion characteristics in cortical gray versus subcortical white matter, and neurodegeneration at chronic stages. We assessed multilineage cell expression changes using single-nucleus RNA sequencing (snRNA-seq) and validated results using large area multiplex fluorescent *in situ* hybridization. We found selective vulnerability and loss of excitatory *CUX2*-expressing projection neurons in upper cortical layers underlying meningeal inflammation; such MS neuron populations showed upregulation of stress pathway genes and long non-coding RNAs. Signatures of stressed oligodendrocytes, reactive astrocytes and activated phagocytosing cells mapped most strongly to the rim of MS plaques. Interestingly, snRNA-seq identified phagocytosing microglia and/or macrophages by their ingestion and perinuclear import of myelin transcripts, confirmed by functional mouse and human culture assays. Our findings indicate lineage- and region-specific transcriptomic changes associated with selective cortical neuron damage and glial activation contributing to MS lesion progression.

Multiple sclerosis (MS) is a progressive neuroinflammatory autoimmune disease affecting about 2.3 million people worldwide[1] with immune-mediated cytotoxic effects on oligodendrocytes (OLs) causing demyelination and focal plaque formation[2-4], accompanied by progressive axonal damage in the affected white matter (WM)[5,6]. Active lesions typically show inflammation and myelin phagocytosis at the rim of a plaque. Extensive cortical gray matter (GM) pathology includes demyelination and damage to the axon, neurite and neuron cell body[7-9], particularly in areas underlying meningeal inflammation with plasma cell infiltration[10-12]. However, whether this process affects all or a subset of cortical neurons is poorly understood[13]. Cell type-specific mechanisms of MS progression, including scar formation with slowly expanding WM lesions[14] and cortical atrophy[15] are poorly understood. Indeed, because MS lesions are heterogeneous in GM versus WM compartments, the underlying pathobiology, and potential for repair, is likely to vary in a region-restricted manner between cortical and subcortical lesion types.

Single-cell transcriptomic techniques are well suited to identify cellular heterogeneity in the human brain[16], and recently they have been applied to individual glial lineages in MS[17,18]. Here, we took a multilineage approach to brain-resident populations (neurons, astrocytes, OLs, microglia) focusing on cortical GM and subcortical WM to better understand molecular, cellular and spatially-restricted substrates of progressive MS pathology. We used frozen human brain samples from MS cases and controls to perform unbiased isolation of nuclei from subcortical and cortical lesion and non-lesion areas followed by single-nucleus RNA-sequencing (snRNA-seq)[17,19,20] and *in situ* validation of RNA gene expression across large anatomical areas. Our results indicate that genes most dysregulated in MS map spatially to vulnerable upper cortical layer neurons and reactive glia at the borders of subcortical MS lesions associated with progression in MS.

Results

snRNA-seq using post-mortem frozen MS tissue reveals cell-type specific molecular changes associated with MS pathogenesis. To analyze cell type-specific gene expression changes in the MS cortex, we used snRNA-seq to profile MS tissue samples that were chosen to capture cortical GM and adjacent subcortical WM lesion areas at various stages of inflammation and demyelination, as well as control tissue from unaffected individuals. We established a pipeline to perform serial sectioning of the entire tissue block to collect tissue covering all areas of lesion and normal-appearing (non-lesion) GM and WM areas, including attached meningeal tissue. Tissue sections were screened by RNA integrity number (RIN) with an *a priori* cut off of 6.5. Using this criterion, 12/19 MS tissue samples screened from 10 individuals and 9/16 samples screened from control individuals were deemed suitable for snRNA-seq processing (**Figure 1a**; **Table S1**). As shown (**Table S1**), the distribution of confounding variables such as age, sex, postmortem interval and RIN was not significantly different between control and MS subjects ($p>0.1$, Mann-Whitney U test).

We then optimized and performed unbiased nuclei isolation using sucrose-gradient ultracentrifugation (**Figure S1a**), followed by single nuclei RNA barcoding (10x Genomics) and subsequent cDNA sequencing (**Figure 1b,** see **Extended Methods** for details). snRNA-seq yielded 48,919 single-nuclei profiles after quality control filtering (**Figure 1b-c**, **Table S2**). Following normalization of data, we applied several independent analysis techniques. Unbiased clustering identified 22 cell clusters (**Figure 1c**; *n.b.,* none comprised nuclei captured from a single MS or control sample). We detected a median of 1,400 genes and 2,400 transcripts per nucleus, with higher numbers of transcripts detected in neuronal versus glial populations (**Figure S1b**). In this study we focused on resident brain cells of neuronal, astrocyte, oligodendroglial and

84 microglial lineages. We annotated cell clusters based on expression of lineage marker genes for
85 excitatory and inhibitory cortical neurons, astrocytes, oligodendrocyte lineage cells and
86 microglia as well as other minor cell populations (**Figure 1d**, **Figure S1e**, **Table S3**)[21].
87 Neuronal subtype markers included interneuron marker *GAD2*, excitatory neuron marker
88 *SCL17A7*, upper layer marker *CUX2*, layer 4 marker *RORB*, deep layer marker *TLE4*, as well as
89 interneuron subtype markers *PVALB*, *SST*, *VIP* and *SV2C*.

90 Comparing normalized numbers of nuclei captured from MS cases and controls, we
91 observed a striking reduction of upper-layer excitatory projection neuron (EN-L2-3A, B)
92 numbers in MS samples with cortical demyelinated lesions (**Figure 1e**). In contrast, numbers of
93 intermediate (EN-L4) and deep-layer (EN-L5-6) excitatory neurons, as well as *THY1/NRGN*-
94 high-expressing pyramidal cells, *VIP*-expressing, somatostatin *(SST*) - and parvalbumin
95 *(PVALB*)-expressing interneurons were similar between MS samples and controls (**Figures 1e-f**).
96 MS-associated genes showed greatest differential expression in EN-L2-3, followed by EN-L4
97 and myelinating OLs (**Figure 1g**). Notably, for EN-L2-3 and OLs, these dramatic transcriptomic
98 changes resulted in separation of these cell types into clusters depending on their origin from MS
99 or control samples (**Figure 1c**). In contrast to EN-L2-3 cells, gene dysregulation was less
100 pronounced in upper layer *VIP*-expressing interneurons (**Figure 1g**). These findings suggested
101 cell type vulnerability in layer 2/3 excitatory *CUX2*-positive neurons.

102

103 **Selective vulnerability of MS *CUX2*-expressing upper layer cortical projection neurons.** We
104 investigated changes in *CUX2*-expressing EN-L2-3 cells in MS lesion pathology using
105 unsupervised pseudotime trajectory analysis to identify dynamic gene expression changes
106 (**Figure 2a**). We found that cell distribution along the trajectory separated control from MS

CUX2-positive cells; interestingly, we found that progression along the trajectory correlated with conventional inflammatory lesion staging and the degree of upper layer cortical demyelination (**Figure 2b, Figures S2c-d)**. For example, *CUX2*-expressing neurons, which localized towards the trajectory end, derived mainly from samples harboring late chronic inactive lesions with extensive subpial demyelination as compared to early acute and chronic-active lesions with less upper cortical demyelination (**Figure 2c)**.

Trajectory analysis highlighted gene ontology (GO) terms (**Figure 2d**) and dynamic upregulation of oxidative stress, mitochondrial dysfunction and cell death pathways suggesting damage of *CUX2*-expressing neurons (**Figure 2e**). Specific dynamically upregulated genes included stress-related and cell death genes (*FAIM2, ATF4, CLU, B2M*), heat-shock response related genes (*HSPH1, HSP90AA1*), protein accumulation and axon degradation associated transcripts (*APP*, *NEFL*, *UBB*), genes linked to energy metabolism and oxidative stress (*COX7C, PKM, PPIA*), as well as long-noncoding (lnc) RNAs *LINC00657 (NORAD*) and *BCYRN1 (BC200)* (**Figure 2e, Figure S2a,Table S4**)[22,23]. Conversely, we noted dynamic downregulation of transcripts associated with mitochondrial energy consumption (*FARS2*), glutamate signaling (*GRIA4*, *GRM5*), potassium/cation homeostasis (*KCNB2, KCNN2, SLC22A10*), neuronal signaling (*NELL1*), axon plasticity (*ROBO1*) and lncRNA *LINC01266* (**Figure 2f**). We observed similar enrichment of cell stress pathways for excitatory neurons from all cortical layers by performing differential expression analysis and comparing control and MS cells in each cell type (**Figure S2b**, **Table S4, Materials and Methods**). However, for cortical interneuron populations, only one GO term associated with protein folding was enriched for genes dysregulated in IN-PVALB and IN-VIP interneurons (**Table S4**). Together, these findings

indicate a gradual transition of *CUX2*-expressing neurons towards a transcriptomic damage signature, that appears to be driven by disease progression and to result in neuronal death.

Loss of *CUX2*-expressing excitatory projection neurons in demyelinated cortical lesions *in situ*. We next used large area spatial transcriptomic (LaST) mapping[24] to validate cell type-specific gene expression changes in a tissue-relevant context. We used chromogenic and multiplex small molecule fluorescent *in situ* hybridization (smFISH) protocols that were optimized to overcome technical difficulties (*e.g.*, high levels of background auto-fluorescence in WM and lipofuscin in neurons) in archival human brain samples (see **Extended Methods**). We achieved favorable signal-to-noise over entire tissue sections for neuronal markers *CUX2* and *SYT1* (neuronal identity marker) combined with immunohistochemistry for myelin oligodendrocyte glycoprotein (MOG) (**Figure 3a**). We also confirmed layer-associated expression of neuronal subtype markers *RORB, THY1*, *TLE4, VIP* and *SST* (**Figure 3a**, **Figure S3a**).

Given snRNA-seq findings above, we investigated expression of co-located upper layer *CUX*2- and *VIP*-expressing neuron populations by smFISH in MS and control tissue sections (**Figures 3b**). We found a significant reduction of *CUX2*-expressing excitatory neurons in both completely and incompletely demyelinated cortical areas (**Figure 3b**). In contrast, adjacent *VIP*-expressing interneuron populations within cortical MS lesion areas remained intact. Of note, meningeal plasma cell infiltration (that predominated over SKAP1^{+} T cells) was a common finding in sulci with underlying upper cortical layer demyelination and loss of *CUX2*-positive neurons (**Figure S3b**)[10,25].

Next, we validated the increase of expression of the cell stress marker *PPIA* (encoding prolyl isomerase cyclophilin A) in MS lesions. *PPIA* was strongly upregulated in correlation with EN-L2-3 trajectory progression (**Figure 2e**) and preferentially upregulated in excitatory upper layer (EN-L2-3 and EN-L4) versus deep layer excitatory (EN-L5-6) and inhibitory (IN-SST) cortical neurons in MS lesion tissue (**Figure S2a**). By smFISH quantification, we found *PPIA* transcripts to be strongly upregulated in both neurons from demyelinated and adjacent normal-appearing cortical lesion areas (**Figure 3c**)[26]. Then, we validated evidence for activation of *NORAD*-Pumilio signaling in cortical MS lesion neurons by chromogenic and fluorescent smFISH. Similar to *PPIA*, *NORAD* was dynamically upregulated along the EN-L2-3 trajectory (**Figure 2e**) and preferentially upregulated in upper cortical excitatory (EN-L2-3 and EN-L4) neurons (**Figure S2a**). *NORAD* has been shown to be activated upon severe genomic stress helping stabilize DNA by binding to PUMILIO and RBMX proteins that are required for neuron survival[22,27]. Although *NORAD* was upregulated in several cell types in MS (**Figure S2a**), strongest upregulation was observed in upper layer excitatory neurons; we validated this finding by analysis of cytoplasmic *NORAD* accumulation in cortical MS lesion neurons as compared to normal-appearing areas with intact myelin (**Figure 3c**). These findings confirm degeneration and selective loss of *CUX2*-expressing upper layer excitatory neurons in cortical MS lesions, while abutting interneurons and other cortical excitatory neuron subtypes were relatively preserved.

Defined macroglial signatures are expressed in spatially distinct cortical and subcortical lesion areas. Prior studies have indicated differential gene expression and functionally diverse properties of reactive astrocytes that can be antagonistic or beneficial to repair after injury[28,29]. We identified astrogliosis by enhanced immunoreactivity for glial fibrillary acidic protein

(GFAP) in regions of subcortical demyelinated WM that did not cross into the demyelinated cortex in MS lesions. The GFAP signature in demyelinated WM overlapped with *CD44*-expressing reactive astrocytes[30], with the strongest expression pattern at the margins of lesions; these astrocytes also showed upregulated *CRYAB* and *MT3* (**Figures S4a-b, Table S3**)[31]. As shown (**Figure 4a, Figure S4a**), *RFX4* expression captures all *SLC1A2*-positive GM and *CD44*-positive WM astrocytes. We also observed downregulation of genes for glutamate (*SLC1A2*, *GLUL*) and potassium homeostasis (*KCNJ10*)[32] in cortical GM astrocytes and confirmed expression of *GPC5*, a marker that co-localizes with *RXF4*-expressing GM astrocytes, in lesion and non-lesion cortical areas *in situ* (**Figure 4a-b, Figure S4a**). Reactive astrocytes at inflammatory chronic active lesion rims also showed strong expression of the transcription factors *BCL6*, *FOS* (encoding *c-FOS*) – associated with astrocyte endothelin receptor type B (*EDNRB*) upregulation – and the lncRNA *LINC01088* (**Figure 4b**, **Figure S4b**)[33]. Thus, spatial transcriptomics revealed distinct expression patterns for cortical versus subcortical reactive astrocytes in the MS lesion microenvironment.

Myelinating OLs characterized by myelin gene expression and the transcription factor *ST18* (**Figure 1d, Figure S4c**) exhibited the third highest number of differentially expressed genes (**Figure 1g**) consistent with vulnerability, enriched stress pathways as shown by GO terms (**Figure S4d**) and a known cell loss of this cell type in MS pathology. Differential gene expression analysis indicated upregulation of genes for heat shock response (*HSP90AA1*), [34]cell stress and death (*FAIM2*, *ATF4*), MHC class I upregulation (*B2M*, *HLA-C*), iron accumulation (ferritin encoding *FTL*, *FTH1*)[34,35] and ubiquitin-mediated protein degradation (*UBB*) as well as the lncRNAs *LINC00657* and *LINC00844* (**Figure 4c-d**, **Figure S4e**). Conversely, we observed downregulation of markers for OL differentiation and myelin synthesis (*BCAS1*, *SGMS1*)[36] and

potassium/cation homeostasis (*KCNJ10*)[32] as well as cell-cell-interaction (*SEMA6A*) and formation of the node of Ranvier (*GLDN*) in MS OLs at lesion borders (**Figure 4c**). In summary, our findings indicate severe cell stress in MS OLs that can be mapped back to periplaque rim areas of subcortical lesions.

Activated and phagocytosing microglial cells can be identified by snRNA-seq and mapped to chronic-active MS lesion rims. We observed a dramatic expansion of microglia in MS samples (**Figure 1e**). In order to identify lesion-specific microglia subtypes, we performed hierarchical clustering of all captured cells with a microglial gene signature (**Figure S5)**. We observed microglial cells with a homeostatic gene expression signature (*P2RY12*, *RUNX1*, *CSF1R*) present in both MS and control samples as well as MS-specific cells with enrichment for transcripts encoding activation markers (*CD14, FTL, MSR1, SPP1*, *APOE)*, complement factors (*C1QA*, *C1QB*, *C1QC*) and MHC-II associated proteins (*CD74*, *HLA-DRB1*, *HLA-DRA*)[18] (**Figure S5a, Table S5**). Moreover, we found microglial cells characterized by enrichment for OL-specific marker genes like *PLP1*, *MBP* and *ST18* (**Figure S4c, Figure S5a, Table S5**). Of note, phagocytosing cells formed an unique cluster characterized by presence of myelin and microglial transcripts (**Figure 1c-d**), suggesting the possibility that ingested myelin transcripts co-purified with nuclei of phagocytosing cells. In addition to those above, genes upregulated in MS microglia (versus controls) were linked to myelin and lipid degradation (*ASAH1*, *ACSL1, DPYD*) (**Figure 5a**). For downregulated genes in MS microglia, among others we found synapse remodeling transcript *SYNDIG1*[37], and potassium channel *KCNQ3* in MS microglia (**Figure 5a**). As shown (**Figure 5a-b, Figure S5, Table S5**), marker genes for microglia reactivity (*CD68*,

CD74, *FTL*, *MSR1*) colocalized with the lineage microglia marker *RUNX1*, and mapped such activated cells to chronic active boundaries of subcortical MS lesions.

To provide functional evidence for putative myelin RNA microglial phagocytosis, we cultured human and mouse microglia exposed to purified myelin from rat brain (**Figure 5c**), which contains myelin transcripts (**Figure S6**). We found significant uptake of myelin and *PLP1* and *MBP* transcripts to intracellular, perinuclear and nuclear compartments of microglia at 1-day post exposure to labeled (pHrodo) myelin. Indeed, ingested *MBP* mRNA was observed in mouse microglia up to 4-days post myelin feeding (**Figure 5c)**. In parallel, we observed morphological changes in phagocytosing mouse microglia, differential upregulation of the activation marker *Cd163*[38] and downregulation of the homeostatic microglia marker *P2ry12*[39]. Such changes in mouse microglia showed parallel gene expression changes in human MS phagocytosing cells by snRNA-seq (**Figure 5c**).

Interactive single-cell web browser to visualize cell-type specific transcriptional changes in MS. We have created an interactive web browser to visualize MS-associated cell-type specific changes (https://ms.cells.ucsc.edu). The web browser allows studying cell-type specific expression levels of individual genes and transcriptomic changes throughout different lesion stages of MS versus control tissues.

Discussion

MS lesions are quite heterogeneous in cortical and subcortical lesion areas with distinct patterns of inflammatory demyelination[13,40,41]. Our findings indicate cell type-specific gene expression changes in regions of cortical neurodegeneration and at the rim of chronic active subcortical lesions involved in progressive MS and cortical atrophy. Results of our snRNA-seq analysis highlight feasibility of the approach in MS and are consistent with findings[17-19]. We validated candidate gene expression using large area spatial transcriptomics in human MS brain.

In this study, we used high-quality archival samples from patients who did not receive modern immune modulatory therapies; thus, they represent more or less the endpoint of the natural disease course with relatively early death of patients (e.g., 30-50 years of age). A limitation of this study is the number MS samples, which could have resulted in under-reporting of certain lineages. Computational analysis of differential gene expression and trajectory analysis of a total of 12 MS and 9 control samples pointed most strongly to the neuronal compartment and indicated dramatic cellular stress and loss of *CUX2*-expressing upper layer excitatory projection neurons in demyelinated and partially remyelinated cortical MS lesions. Such lesions underlie sustained meningeal inflammation with predominant plasma B cell infiltration, highlighting the importance of B cells in progressive MS[10,11]. These findings suggest a mechanism of cortical atrophy in progressive MS that is predicted to benefit from B cell depleting therapies[42,43]. Markers of stressed upper layer excitatory projection neurons included *PPIA* (encoding cyclophilin A), the lnc RNA *NORAD* implicating the Pumilio pathway and other cellular stress pathways related to protein degradation, heat shock response and metabolic exhaustion as critical determinants of neuronal survival[44-46]. Notably, while most transcriptional changes and neuronal cell loss took place in demyelinated regions, we also observed abnormal

gene expression features (e.g., *PPIA*) in normal-appearing cortical areas suggesting a gradient of pathology[47]. Surprisingly, although we observed an increase in differentially expressed genes including cell stress pathways in inhibitory and other excitatory cortical neuron subsets[11], we found upper layer projection neurons to be mostly damaged in MS. While it is possible that *CUX2*-expressing projection neurons are damaged by both sustained meningeal inflammation and retrograde axon pathology from juxtacortical WM lesions, another common lesion site in MS[41], additional intrinsic factors might account for their lack of resilience, especially when one considers that neighboring inhibitory and excitatory neurons of the cortex showed relatively little cell loss.

Recent studies used MS lesion single-nuclei and single-cell RNA-seq to study the OL[17] and microglia[18] lineage focusing on WM lesions and found heterogeneity in both subsets pointing towards specific glial subsets linked to MS pathobiology. Here, we show the feasibility and utility of high-resolution large-area spatial transcriptomics to map dysregulated genes in multiple lineages back to the relevant human brain tissue studying both cortical and subcortical lesion and non-lesion areas for insights into disease single-cell pathology. Transcriptomic changes associated with oligodendroglial, microglial and astrocyte activation mapped predominantly to the rim areas of chronic active subcortical lesions[14,48]. Notably, both stressed myelinating OLs and upper layer cortical projection neurons upregulated genes for self-antigen presentation to immune cells (*B2M, HLA-C*) suggesting cell-intrinsic processes that might promote ongoing degeneration and inflammation, in agreement with others[49,50]. At subcortical lesion rims, we found that MS OLs showed molecular changes indicating both cellular degeneration and iron overload[34,35].

In another example of MS lineage spatial diversity, we detected distinct transcripts in cortical versus subcortical lesion astrocytes, providing insight into the role of tissue microenvironment in regions that show differential extent of pathology. Further, we found that snRNA-seq can distinguish phagocytosing cells in MS because of myelin transcript import into peri-nuclear structures or the nucleus itself. Future work is needed to determine whether this biology is beneficial or detrimental in disease course, for example by exacerbating inflammation in MS. In summary, multilineage and spatial gene expression analysis indicates cell type-specific cortical neurodegeneration and glial activation patterns involved in regions of MS lesion progression.

Acknowledgements

We thank Dr. Djordje Gveric for selecting and providing human brain samples from the UK Multiple Sclerosis Tissue Bank, funded by the Multiple Sclerosis Society of Great Britain and Northern Ireland. We thank the NIH NeuroBioBank at the University of Maryland, School of Medicine, in particular Dr. Alexandra LeFevre for help with obtaining tissue samples and sample information. We thank Dr. Jason Cyster (University of California, San Francisco, USA), Dr. Daniel Reich (National Institutes of Health, Bethesda, USA) and Dr. Sarah Teichmann (Wellcome Sanger Institute, Hinxton, UK) for helpful comments. We thank Irina Pshenichnaya (University of Cambridge, UK) for expert technical assistance. We thank Anna Hupalowska for assistance with figure illustrations. L.S. was supported by postdoctoral fellowships from the German Research Foundation (DFG, SCHI 1330/1-1) and the National Multiple Sclerosis Society Dave Tomlinson Research Fund (NMSS, FG-1607-25111). D.V. was supported by a BOLD & BASIC fellowship from the Quantitative Biosciences Institute at University of California, San Francisco. S.M. was supported by postdoctoral fellowships from the European Molecular Biology Organization (EMBO, ALTF_393-2015) and the DFG (MA 7374/1-1). A.B. was supported by a postdoctoral fellowship (F32NS103266) from the National Institutes of Health (NIH). D.H.R. is a Paul G Allen Frontiers Group Distinguished Investigator. The study was supported by a Pilot Research Grant from the NMSS (PP-1609-25953; L.S., D.H.R.), the Adelson Medical Research Foundation (D.H.R., D.P.S., R.J.M.F.), the UK Multiple Sclerosis Society (R.R., R.J.M.F.), the Loulou Foundation (D.H.R.), the NIHR Cambridge Biomedical Research Center (D.H.R.), and grants from the NIH/NINDS (NS040511 to D.H.R., R35NS097305 to A.R.K.), European Research Council and the Wellcome Trust (to D.H.R).

Author contributions

L.S., D.V., A.R.K. and D.H.R. designed, coordinated and interpreted all studies and wrote the manuscript. L.S. performed immunohistochemical stainings and did histopathological assessment and staging of control and MS samples. L.S., D.V. and D.J. performed nuclei isolation and capturing experiments as well as cDNA library preparations. D.V. analyzed sequencing data and performed regression analysis related to differential gene expression and cluster analysis. S.H. performed and analyzed multiplex fluorescent ISH experiments. M.K. analyzed sequencing data and performed trajectory pseudotime and signaling pathway analysis. S.W. conducted myelin-microglia engulfment assays and performed subsequent IHC, *in situ* hybridization and qPCR experiments. J.H.S., A.Y. and M.S. carried out human myelin-microglia engulfment assays and subsequent ISH experiments. L.S., D.J., S.V. and S.M. performed chromogenic and fluorescent *in situ* hybridization experiments. B.T. and N.G. performed computational analysis of sequencing data and helped with nuclei isolation experiments. A.B. and J.B.E. wrote and modified computational scripts for analysis of single-cell data. O.A.B. supervised multiplex fluorescent ISH experiments. R.J.M.F. supervised human myelin-microglia engulfment assays. M.H. generated the single-cell web browser to visualize control and MS sequencing data. R.R. and L.S. selected and characterized control and MS cases used in this study. R.R. analyzed findings related to neuronal and meningeal pathology in MS. D.P.S. analyzed microglia data sets and supervised mouse myelin-microglia engulfment assays. M.F. analyzed findings related to neuron pathology and supervised computational trajectory and signaling pathways analyses. L.R.S. analyzed findings related to immune and glial cell subsets and supervised chromogenic ISH experiments. All coauthors read, revised and approved the manuscript. D.H.R. and A.R.K. supervised all experiments.

Competing interests

The authors state no relevant competing interests or disclosures.

Figure legends

Figure 1. Experimental approach and characteristics of snRNA-seq using frozen MS tissue. (**a**) Overview of control, cortical and subcortical MS lesion types captured in the current study (GM = cortical gray matter, WM = subcortical white matter, DM = demyelination, NA = normal appearing GM/WM). (**b**) Experimental approach to isolating nuclei from postmortem snap-frozen brain samples of MS and control patients. (**c**) Overview of cell types from individual samples (left), belongings to separate cell-type specific clusters (center) and contribution of control (n=9) and MS (n=12) samples to individual clusters (right). Note separation of EN-L2-3 (excitatory upper layer neurons) and OL (myelinating oligodendrocytes) cells into MS-specific disease clusters EN-L2-3-B and OL-B/C. (**d**) Marker gene expression characterizing neurons, astrocytes, oligodendrocytes and microglia. (**e**) Bar chart showing contributions of normalized cell numbers of control and MS samples to major cell-type specific clusters. The observed trend of EN-L2-3-A cell enrichment and concominant decrease in EN-L2-3-B in control samples over MS was not statistically significant. (**f**) Neuron subtype specific loss of upper layer (EN-L2-3) but not intermediate (EN-L4), deep (EN-L5-6) or VIP-expressing inhibitory (IN-VIP) neurons based on normalized cell numbers. (**g**) Differential gene expression analysis shows highest number of dysregulated genes in EN-L2-3 followed by EN-L4 cells and OLs. Note least differentially expressed genes in IN-SST (SST-expressing interneurons) and OPCs. Mann-Whitney tests were performed in **e** and **f**; *$P \leq 0.05$. Data are presented as mean ± s.e.m.

Figure 2. Pseudotime trajectory analysis of upper layer excitatory projection neurons. (**a**) Trajectory analysis of EN-L2-3 cells based on cell-type specific *CUX2* expression (upper left). Unsupervised pseudotime trajectories within the EN-L2-3 (upper right) cluster reflect separation

into cellular origin from control and MS samples (lower left) and followed inflammatory lesion stages (lower right). (**b**) EN-L2-3 pseudotime trajectories separate cells from control and MS (upper left) and control from inflammatory lesion stages (center left) and also reflect loss of normalized EN-L2-3 numbers (lower left). Strongest association with EN-L2-3 trajectories found for upper cortical layer demyelination (upper right) versus deep cortical layer (center right) and subcortical demyelination (lower right). (**c**) Note selective enrichment of dysregulated genes in EN-L2-3 cells from samples with late chronic inactive lesions as compared to acute/chronic-active and control samples. (**d**) Visualization of GO terms enriched for genes that are upregulated in EN-L2-3 in a pseudotime-dependent manner. Note enrichment of severe cell stress processes. (**e**) Trajectory-dependent upregulated (left) and downregulated (right) EN-L2-3 genes of interest.

Figure 3. Cellular and molecular neuronal pathology in cortical MS lesions. (**a**) tSNE plots for neuron subtype specific expression of *CUX2*, *VIP* and *TLE4* (left). Large area spatial transcriptomics (LaST) showing layer-specific expression of neuronal *CUX2* in demyelinated lesion versus non-lesion areas (center left). Schematic illustrates cortical layer-specific neuron subtype diversity (center). Confirmation of *CUX2* and *VIP* expression in upper and *TLE4* in deep cortical layers by smFISH (center right). Co-expression studies with *SYT1* confirm neuronal expression of *CUX2*, *VIP* and *TLE4* (black arrowheads). (**b**) Combined MOG immunohistochemistry (IHC) and *CUX2 in situ* hybridization shows selected loss of *CUX2*-positive neurons in demyelinated area directly underlying meningeal inflammation (upper left). Note selective loss of *CUX2*- (center) but not *VIP*- (right) expressing upper layer neurons in subpial demyelination (white arrowheads), confirmed by quantification in demyelinated

(DMGM, *CUX2/VIP*: n = 8/8) versus incomplete demyelinated (IDMGM, *CUX2/VIP*: n = 7/7), normal-appearing (NAGM, *CUX2/VIP*: n = 5/5) and control (ctrl, *CUX2/VIP*: n = 5/4) upper cortical gray matter areas from different tissue blocks (bottom left). ANOVA with Kruskal Wallis multiple comparison tests were performed; *P ≤ 0.05. (**c**) Strong and gradual upregulation of *PPIA* encoding cyclophilin A in cortical neurons from both demyelinated (n = 4) and normal-appearing (n = 4) adjacent cortical lesion areas as compared to control gray matter (n = 3) (left, white encircled areas indicate perinuclear areas of *PPIA* quantification). Striking upregulation and cytoplasmic accumulation of the long non-coding RNA *LINC00657 (NORAD*) in neurons of demyelinated (n = 4) cortical lesion areas as compared to normal-appearing (n = 4) and control areas (n = 3) (right, black arrowheads). ANOVA with Tukey's multiple comparison tests were performed in **c**; *P ≤ 0.05. Data are presented as mean ± s.e.m.

Figure 4. Transcriptomic changes in astrocytes and myelinating oligodendrocytes in cortical and subcortical MS lesions. (**a**) Differential downregulation of homeostatic protoplasmic astrocyte genes *SLC1A2* and *GPC5* in MS, as opposed to differential upregulation of astroglial *GFAP* and *CD44* in MS (upper left). LaST confirms downregulation of *SLC1A2* (associated with *RFX4*-expressing NAGM astrocytes, bottom left, white arrowheads) in cortical demyelination underlying meningeal inflammation, whereas *CD44* shows ubiquitous expression in WM areas (associated with *RFX4*-expressing NAWM and PPWM [periplaque white matter] astrocytes, center left, white arrowheads). Note strong upregulation of astroglial *CD44* at the chronic active lesion rim in enlarged area (b1, center right). Co-expression studies confirm *CD44* and *GPC5* co-expression with pan-astrocyte marker *RFX4* (black arrowheads). Note selective *CD44* expression/upregulation in fibrous/reactive WM astrocytes and *GPC5* enrichment in

protoplasmic cortical GM astrocytes (black arrowheads; right). White star indicates central blood vessel in lesion core. (**b**) Downregulation of glutamine synthetase (*GLUL*) and potassium channel KIR4.1 (*KCNJ10*) in MS astrocytes (left). Note differential upregulation of *BCL6* and *FOS* encoding transcription factors in reactive astrocytes mapped to the lesion rim (center, black arrowheads). The novel lnc RNA *LINC01088* is specifically expressed in fibrous/reactive WM astrocytes (right, black arrowhead). (**c**) tSNE plots for selected upregulated (top) and downregulated (bottom) genes in MS OLs linked to several cell stress pathways (upregulation) and OL function in myelin biosynthesis and axon maintenance. (**d**) Ferritin transcripts *FTL* and *FTH1* are strongly upregulated in *PLP1*-expressing OLs at iron-laden lesions rims (left, black arrowheads). Note also differential upregulation of MHC class I transcripts *B2M* and *HLA-C* in *PLP1*-expressing OLs at PPWM areas (right; yellow arrowheads [white arrowheads mark OLs without *B2M* ISH signals in NAWM]).

Figure 5. Transcriptomic changes in activated and phagocytosing microglia subsets. (a) tSNE plots for selected upregulated genes in activated MS microglia linked to OL/myelin phagocytosis and enzymatic breakdown (left) as well as to microglia/macrophage activation and iron metabolism/uptake (center); note selective downregulation of genes encoding for synapse function (*SYNDIG1*) and potassium homeostasis (*KCNQ3*) (right). (**b**) LaST 3D rendering shows complex subcortical WM lesions of different inflammatory stages by combining *MBP* smFISH with CD68 IHC, white arrowheads indicate $CD68^+$ cells with MBP^+ ISH signals; note colocalization of *MBP* transcripts in subset of CD68-positive cells co-expressing MHC-II related *CD74* and canonical transcription factor gene *RUNX1* (left-center left, white arrowheads). CD68 IHC identifies focal WM lesion with central blood vessel (black star) (center upper right). Note

selective enrichment of microglia marker gene *MSR1* at lesion rims (lower right), co-expressed with *RUNX1* (lower right, black arrowheads) and associated with *FTL* expression (upper right, black arrowheads). (**c**) Human (upper left) and mouse (upper center right) myelin-microglia culture engulfment assay confirming ingestion of *MBP* and *PLP1* transcripts from rat myelin preparations and showing localization to nuclear and perinuclear spaces (white arrowheads). Microglia cells were labelled by pHrodo (human) and Iba1/CD68 (mouse) and LMNA/C and DAPI were used to stain nuclei. Schematic illustrates predicted mode of action showing myelin phagocytosis and uptake into (peri-)nuclear microglial spaces by microglia (upper right). Uptake and persistence of myelin engulfment up to 4 days after ingestion in mouse microglia cells confirmed by smFISH quantification for subcellular *MBP* transcripts (4 independent cultures each derived from a different animal; lower left); note differential upregulation of macrophage activation marker *Cd163* and downregulation of homeostatic marker *P2ry12* in myelin-phagocytosing cells reflecting expression patterns in human MS microglia by snRNA-seq (6 independent cultures each derived from a different animal; lower right). Mann-Whitney tests were performed; *$P \leq 0.05$. Data are presented as mean ± s.e.m.

Figure S1. Sample and disease contribution of cell types captured by snRNA-seq. (a) Nuclei suspension after ultracentrifugation and before capturing by 10X Genomics confirming DAPI nuclear counterstaining with presence of smaller and larger $DAPI^+$ nuclei. Note that larger nuclei are co-stained with anti-NeuN antibody confirming neuronal origin (white arrowheads) **(b)** Colored t-SNE plots showing numbers of genes (left) and UMIs (right) per captured nuclei from control and MS samples. **(c)** Colored t-SNE plot visualizing nuclei from different lesion stages based on classic pathological MS lesion staging. **(d)** Colored t-SNE plots visualizing nuclei from

samples with different levels of upper and deep layer cortical demyelination as well as subcortical demyelination. **(e)** Cell-type specific marker genes for OL progenitor cells, stromal cells including pericytes, endothelial cells, and leukocytes.

Figure S2. Molecular changes in cortical neuron subtypes in MS lesions. (a) *NORAD* and *PPIA* expression patterns in cortical neurons and selected glial subtypes. Note baseline expression of *NORAD* and *PPIA* in neuronal versus glial subtypes and preferential upregulation of both *NORAD* and *PPIA* in upper cortical layer excitatory neurons (EN-L2-3 and EN-L4) in MS lesion tissue versus deep cortical layer excitatory and inhibitory neurons (EN-L5-6 and IN-SST). **(b)** Visualization of enriched GO terms in EN-L2-3, EN-L4 and EN-L5-6 cells based on differential gene expression analysis.

Figure S3. Cortical neuron and lymphocyte subtype analysis in MS lesions. (a) tSNE plots for neuron subtype specific expression of *RORB*, *THY1*, *NRGN*, *SST*, *SV2C* and *PVALB* (left). LaST showing layer-specific expression of neuronal *RORB* in intermediate cortical layer 4 and widespread expression of pyramidal neuron marker *THY1* with enrichment in layer 5; note that *SST*-expressing interneurons preferentially map to deep cortical layers. Co-expression studies with *SYT1* confirm neuronal expression of *RORB*, *THY1* and *SST* (black arrowheads). (**b**) Heatmap with hierarchical clustering of lymphocyte-associated transcripts allowing sub clustering of lymphocytes in T cells, B cells and plasma cells based on marker gene expression (upper left). tSNE plots for typical B/plasma cell and T cell marker genes enriched in lymphocyte clusters (upper right). IHC for T cell marker SKAP1 (black arrowheads mark $SKAP1^+$ T cells) together with spatial transcriptomics for B cell-associated *IGHG1* encoding

immunoglobulin G1 (IgG1) (magenta-colored arrowheads; lower left); note preferential clustering of plasma cell-associated MZB1^{+} and *IGHG1*-expressing B cells (white arrowheads, lower right) in inflamed meningeal tissue versus mixed T and B cell infiltration in perivascular cuffs of subcortical lesions (lower panels). One caveat to these findings is the relatively small number of MS cases samples, which limited our ability to cluster T cell populations.

Figure S4. Astrocyte and oligodendrocyte cluster analysis and spatial transcriptomics in MS lesions. (**a**) Differential spatial expression patterns of astroglial GFAP in subcortical versus cortical demyelination (left); tSNE plots visualizing astrocyte specific genes corresponding to all (*RFX4*) protoplasmic (*SLC1A2*, *GPC5*) and fibrous/reactive astrocytes (*GFAP*, *CD44*). Quantification of *RFX4*$^{+}$ ISH signals per nuclei in GM and WM of control samples validates *RFX4* as a canonical astrocyte marker; quantification of *GPC5*$^{+}$ and *CD44*$^{+}$ ISH signals per *RFX4*$^{+}$ astrocytes confirms validates *GPC5* as protoplasmic GM and *CD44* as fibrous WM marker. Mann-Whitney tests were performed; *P ≤ 0.05. Data are presented as mean ± s.e.m. (**b**) Upregulation of astroglial *CRYAB*, *MT3* (black arrowheads) and endothelin type B receptor transcript *EDNRB* (white arrowhead) in reactive astrocytes in subcortical lesions. (**c**) tSNE plots showing OL-specific expression of myelin genes *MBP* and *CNP* as well as transcription factor *ST18*; note co-expression of *ST18* with PLP in control WM by ISH. (**d**) Visualization of enriched GO terms in myelinating OLs based on differential gene expression analysis. (**e**) Co-expression spatial transcriptomic studies confirming upregulation of heat shock protein 90 transcript *HSP90AA1* in both progenitor (*PDGFRA*-expressing) and myelinating (*PLP1*-expressing) OLs at lesion rims (PPWM, black arrowheads).

Figure S5. Cluster analysis of activated and phagocytosing microglia subtypes. Hierarchical cluster analysis identifies several homeostatic and activated MS-specific microglia subtypes according to inflammatory lesion stages allowing transcriptomic staging of microglia subtypes. Clusters with enriched genes are marked and annotated a-f (see **Table S5** for gene lists). Note that phagocytosing cells are identified by presence of OL/myelin genes (cluster "f" on bottom of heatmap).

Figure S6. PCR for rat *Mbp* from myelin preparation. (**a**) Coomassie stain of brain homogenate (Hom.) and purified myelin (P.M.) from adult rat brain CNS prepared as described in extended methods (left). Western blots for myelin basic protein (MBP), myelin oligodendrocyte glycoprotein (MOG), synaptophysin (Syp.) and neurofilament heavy molecular weight (NF-H) (center). PCRs of myelin basic protein (Mbp) and synaptophysin (Syp.) transcripts in brain homogenate and purified myelin fractions (right). (**b**) Densitometric quantification of n = 4 for Coomassie (total protein) Western blots and PCRs shown in a – c in purified myelin fractions normalized to homogenates.

Table S1. Characteristics of MS and control patient samples included in the study. * = NIH tissue bank samples; GM = cortical gray matter; WM = subcortical white matter; DM = demyelination; PMI = postmortem interval; RIN = RNA integrity number; PP = primary-progressive; SP = secondary-progressive; NA = not applicable; *Inflammatory-demyelinating stage (based on presence of phagocytes and lesion rim inflammation according to largest lesion if more than one lesion present on tissue block); fraction of reads in rells refers to the CellRanger

output after 10x Genomics data analysis and serves as a quality control measure for nuclei capture.

Table S2. Metadata for single nuclei profiles included in the study, as well as pseudotime trajectories for EN-L2-3 neurons.

Table S3. List of unbiased marker genes for each cell type.

Table S4. List of differentially expressed genes and trajectory-dependent EN-L2-3 genes.

Table S5. List of microglial cluster genes based on hierarchical cluster analysis. Note that genes shown in Figure S5 are highlighted in red.

References

1 Collaborators, G. D. a. I. I. a. P. Global, regional, and national incidence, prevalence, and years lived with disability for 310 diseases and injuries, 1990-2015: a systematic analysis for the Global Burden of Disease Study 2015. *Lancet* **388**, 1545-1602, doi:10.1016/S0140-6736(16)31678-6 (2016).

2 Reich, D. S., Lucchinetti, C. F. & Calabresi, P. A. Multiple Sclerosis. *New England Journal of Medicine* **378**, 169-180, doi:10.1056/NEJMra1401483 (2018).

3 Hemmer, B., Kerschensteiner, M. & Korn, T. Role of the innate and adaptive immune responses in the course of multiple sclerosis. *Lancet neurology* **14**, 406-419, doi:10.1016/S1474-4422(14)70305-9 (2015).

4 Lassmann, H. Multiple Sclerosis Pathology. *Cold Spring Harbor perspectives in medicine* **8**, a028936, doi:10.1101/cshperspect.a028936 (2018).

5 Trapp, B. D. *et al.* Axonal transection in the lesions of multiple sclerosis. *The New England journal of medicine* **338**, 278-285, doi:10.1056/NEJM199801293380502 (1998).

6 Schirmer, L., Antel, J. P., Brück, W. & Stadelmann, C. Axonal loss and neurofilament phosphorylation changes accompany lesion development and clinical progression in multiple sclerosis. *Brain pathology (Zurich, Switzerland)* **21**, 428-440, doi:10.1111/j.1750-3639.2010.00466.x (2011).

7 Peterson, J. W., Bo, L., Mork, S., Chang, A. & Trapp, B. D. Transected neurites, apoptotic neurons, and reduced inflammation in cortical multiple sclerosis lesions. *Annals of neurology* **50**, 389-400 (2001).

8 Friese, M. A., Schattling, B. & Fugger, L. Mechanisms of neurodegeneration and axonal dysfunction in multiple sclerosis. *Nat Rev Neurol* **10**, 225-238, doi:10.1038/nrneurol.2014.37 (2014).

9 Mahad, D. H., Trapp, B. D. & Lassmann, H. Pathological mechanisms in progressive multiple sclerosis. *Lancet neurology* **14**, 183-193, doi:10.1016/S1474-4422(14)70256-X (2015).

10 Magliozzi, R. *et al.* Meningeal B-cell follicles in secondary progressive multiple sclerosis associate with early onset of disease and severe cortical pathology. *Brain : a journal of neurology* **130**, 1089-1104, doi:10.1093/brain/awm038 (2007).

11 Magliozzi, R. *et al.* A Gradient of neuronal loss and meningeal inflammation in multiple sclerosis. *Annals of neurology* **68**, 477-493, doi:10.1002/ana.22230 (2010).

12 Lucchinetti, C. F. *et al.* Inflammatory cortical demyelination in early multiple sclerosis. *The New England journal of medicine* **365**, 2188-2197, doi:10.1056/NEJMoa1100648 (2011).

13 Trapp, B. D. *et al.* Cortical neuronal densities and cerebral white matter demyelination in multiple sclerosis: a retrospective study. *Lancet neurology* **17**, 870-884, doi:10.1016/S1474-4422(18)30245-X (2018).

14 Dal-Bianco, A. *et al.* Slow expansion of multiple sclerosis iron rim lesions: pathology and 7 T magnetic resonance imaging. *Acta neuropathologica* **133**, 25-42, doi:10.1007/s00401-016-1636-z (2017).

15 Mainero, C. *et al.* A gradient in cortical pathology in multiple sclerosis by in vivo quantitative 7 T imaging. *Brain : a journal of neurology* **138**, 932-945, doi:10.1093/brain/awv011 (2015).

16 Ecker, J. R. *et al.* The BRAIN Initiative Cell Census Consortium: Lessons Learned toward Generating a Comprehensive Brain Cell Atlas. *Neuron* **96**, 542-557, doi:10.1016/j.neuron.2017.10.007 (2017).
17 Jäkel, S. *et al.* Altered human oligodendrocyte heterogeneity in multiple sclerosis. *Nature* **566**, 543-547, doi:10.1038/s41586-019-0903-2 (2019).
18 Masuda, T. *et al.* Spatial and temporal heterogeneity of mouse and human microglia at single-cell resolution. *Nature* **566**, 388-392, doi:10.1038/s41586-019-0924-x (2019).
19 Lake, B. B. *et al.* Neuronal subtypes and diversity revealed by single-nucleus RNA sequencing of the human brain. *Science (New York, N.Y.)* **352**, 1586-1590, doi:10.1126/science.aaf1204 (2016).
20 Habib, N. *et al.* Massively parallel single-nucleus RNA-seq with DroNc-seq. *Nature Methods* **14**, 955-958, doi:10.1038/nmeth.4407 (2017).
21 Lodato, S. & Arlotta, P. Generating neuronal diversity in the mammalian cerebral cortex. *Annual review of cell and developmental biology* **31**, 699-720, doi:10.1146/annurev-cellbio-100814-125353 (2015).
22 Lee, S. *et al.* Noncoding RNA NORAD Regulates Genomic Stability by Sequestering PUMILIO Proteins. *Cell* **164**, 69-80, doi:10.1016/j.cell.2015.12.017 (2016).
23 Mus, E., Hof, P. R. & Tiedge, H. Dendritic BC200 RNA in aging and in Alzheimer's disease. *Proc Natl Acad Sci U S A* **104**, 10679-10684, doi:10.1073/pnas.0701532104 (2007).
24 Bayraktar, O. A. *et al.* Single-cell in situ transcriptomic map of astrocyte cortical layer diversity. *bioRxiv*, 432104, doi:10.1101/432104 (2018).
25 Machado-Santos, J. *et al.* The compartmentalized inflammatory response in the multiple sclerosis brain is composed of tissue-resident CD8+ T lymphocytes and B cells. *Brain : a journal of neurology* **141**, 2066-2082, doi:10.1093/brain/awy151 (2018).
26 Pasetto, L. *et al.* Targeting Extracellular Cyclophilin A Reduces Neuroinflammation and Extends Survival in a Mouse Model of Amyotrophic Lateral Sclerosis. *Journal of Neuroscience* **37**, 1413-1427, doi:10.1523/JNEUROSCI.2462-16.2016 (2017).
27 Munschauer, M. *et al.* The NORAD lncRNA assembles a topoisomerase complex critical for genome stability. *Nature* **561**, 132-136, doi:10.1038/s41586-018-0453-z (2018).
28 Liddelow, S. A. *et al.* Neurotoxic reactive astrocytes are induced by activated microglia. *Nature* **541**, 481-487, doi:10.1038/nature21029 (2017).
29 Anderson, M. A. *et al.* Astrocyte scar formation aids central nervous system axon regeneration. *Nature*, doi:10.1038/nature17623 (2016).
30 Chang, A. *et al.* Cortical remyelination: a new target for repair therapies in multiple sclerosis. *Annals of neurology* **72**, 918-926, doi:10.1002/ana.23693 (2012).
31 Ousman, S. S. *et al.* Protective and therapeutic role for alphaB-crystallin in autoimmune demyelination. *Nature* **448**, 474-479, doi:10.1038/nature05935 (2007).
32 Schirmer, L. *et al.* Differential loss of KIR4.1 immunoreactivity in multiple sclerosis lesions. *Annals of neurology* **75**, 810-828, doi:10.1002/ana.24168 (2014).
33 Gadea, A., Schinelli, S. & Gallo, V. Endothelin-1 regulates astrocyte proliferation and reactive gliosis via a JNK/c-Jun signaling pathway. *Journal of Neuroscience* **28**, 2394-2408, doi:10.1523/JNEUROSCI.5652-07.2008 (2008).
34 Hametner, S. *et al.* Iron and neurodegeneration in the multiple sclerosis brain. *Annals of neurology* **74**, 848-861, doi:10.1002/ana.23974 (2013).

35 Popescu, B. F. *et al.* Pathogenic implications of distinct patterns of iron and zinc in chronic MS lesions. *Acta neuropathologica* **134**, 45-64, doi:10.1007/s00401-017-1696-8 (2017).
36 Fard, M. K. *et al.* BCAS1 expression defines a population of early myelinating oligodendrocytes in multiple sclerosis lesions. *Science translational medicine* **9**, eaam7816, doi:10.1126/scitranslmed.aam7816 (2017).
37 Kalashnikova, E. *et al.* SynDIG1: An Activity-Regulated, AMPA- Receptor-Interacting Transmembrane Protein that Regulates Excitatory Synapse Development. *Neuron* **65**, 80-93, doi:10.1016/j.neuron.2009.12.021 (2010).
38 Guo, L. *et al.* CD163+ macrophages promote angiogenesis and vascular permeability accompanied by inflammation in atherosclerosis. *J Clin Invest* **128**, 1106-1124, doi:10.1172/JCI93025 (2018).
39 Zrzavy, T. *et al.* Loss of 'homeostatic' microglia and patterns of their activation in active multiple sclerosis. *Brain : a journal of neurology* **140**, 1900-1913, doi:10.1093/brain/awx113 (2017).
40 Lucchinetti, C. *et al.* Heterogeneity of multiple sclerosis lesions: implications for the pathogenesis of demyelination. *Annals of neurology* **47**, 707-717 (2000).
41 Haider, L. *et al.* The topograpy of demyelination and neurodegeneration in the multiple sclerosis brain. *Brain : a journal of neurology* **139**, 807-815, doi:10.1093/brain/awv398 (2016).
42 Hauser, S. L. *et al.* B-cell depletion with rituximab in relapsing-remitting multiple sclerosis. *The New England journal of medicine* **358**, 676-688, doi:10.1056/NEJMoa0706383 (2008).
43 Montalban, X. *et al.* Ocrelizumab versus Placebo in Primary Progressive Multiple Sclerosis. *The New England journal of medicine* **376**, 209-220, doi:10.1056/NEJMoa1606468 (2017).
44 Haider, L. *et al.* Oxidative damage in multiple sclerosis lesions. *Brain : a journal of neurology* **134**, 1914-1924, doi:10.1093/brain/awr128 (2011).
45 Campbell, G. R. *et al.* Mitochondrial DNA deletions and neurodegeneration in multiple sclerosis. *Annals of neurology* **69**, 481-492, doi:10.1002/ana.22109 (2011).
46 Fischer, M. T. *et al.* Disease-specific molecular events in cortical multiple sclerosis lesions. *Brain : a journal of neurology* **136**, 1799-1815, doi:10.1093/brain/awt110 (2013).
47 Carassiti, D. *et al.* Neuronal loss, demyelination and volume change in the multiple sclerosis neocortex. *Neuropathol Appl Neurobiol* **44**, 377-390, doi:10.1111/nan.12405 (2018).
48 Absinta, M. *et al.* Persistent 7-tesla phase rim predicts poor outcome in new multiple sclerosis patient lesions. *J Clin Invest* **126**, 2597-2609, doi:10.1172/JCI86198 (2016).
49 Falcão, A. M. *et al.* Disease-specific oligodendrocyte lineage cells arise in multiple sclerosis. *Nat Med* **24**, 1837-1844, doi:10.1038/s41591-018-0236-y (2018).
50 Kirby, L. *et al.* Oligodendrocyte Precursor Cells Are Co-Opted by the Immune System to Cross-Present Antigen and Mediate Cytotoxicity. *bioRxiv*, 461434, doi:10.1101/461434 (2018).

a

MS cortico-subcortical lesion pathology

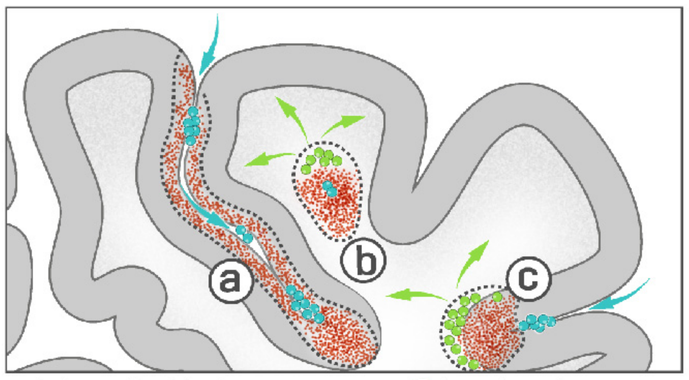

a. intracortical lesion
b. subcortical lesion
c. leukocortical lesion

lymphocytes
activated microglia
demyelinated lesion

Leukocortical lesion
Subcortical lesion

Luxol fast blue myelin stain

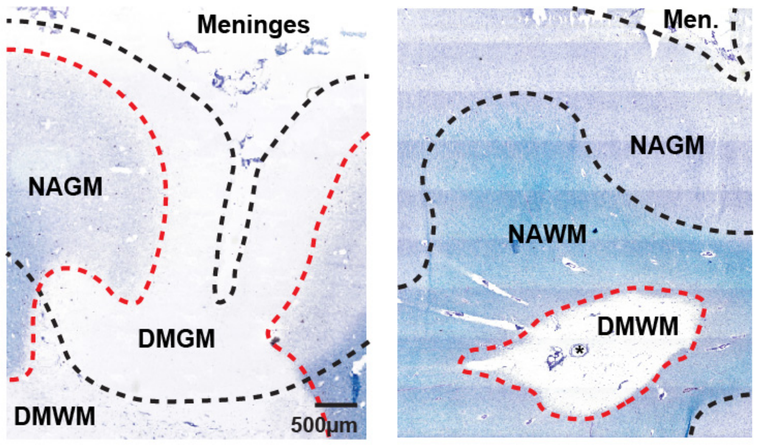

b

snRNA-seq procedure

Tissue selection
Ultracentrifugation

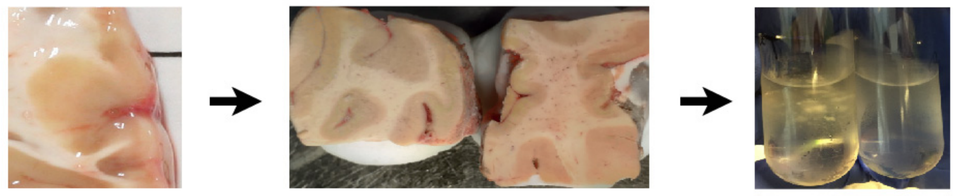

Nuclei capturing
RNA-seq

c

Sample distribution to cell clusters

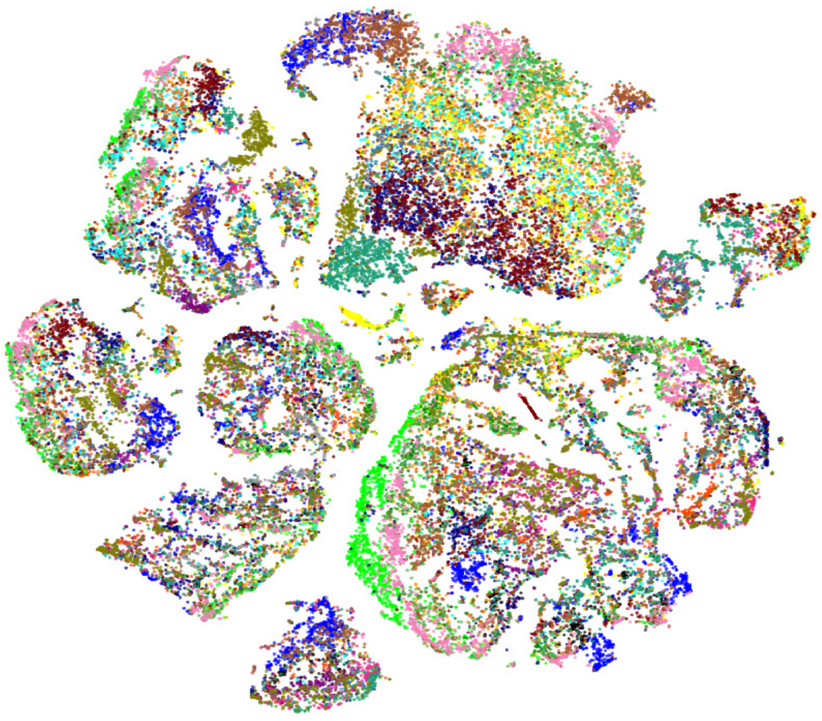

Unbiased snRNA-seq clustering

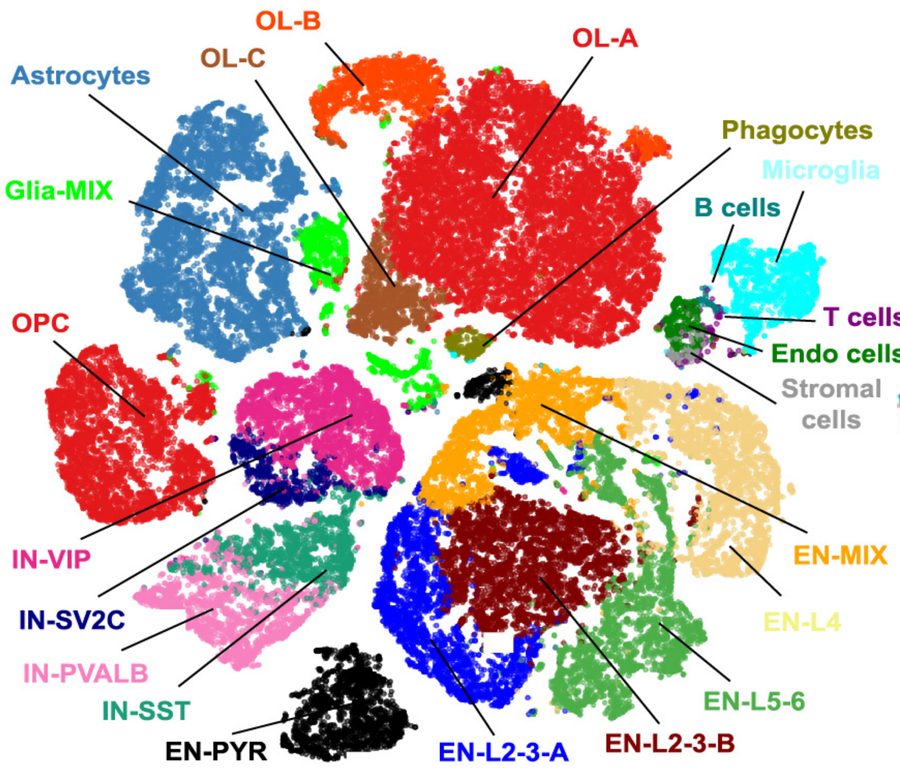

Ctrl vs MS nuclei clustering

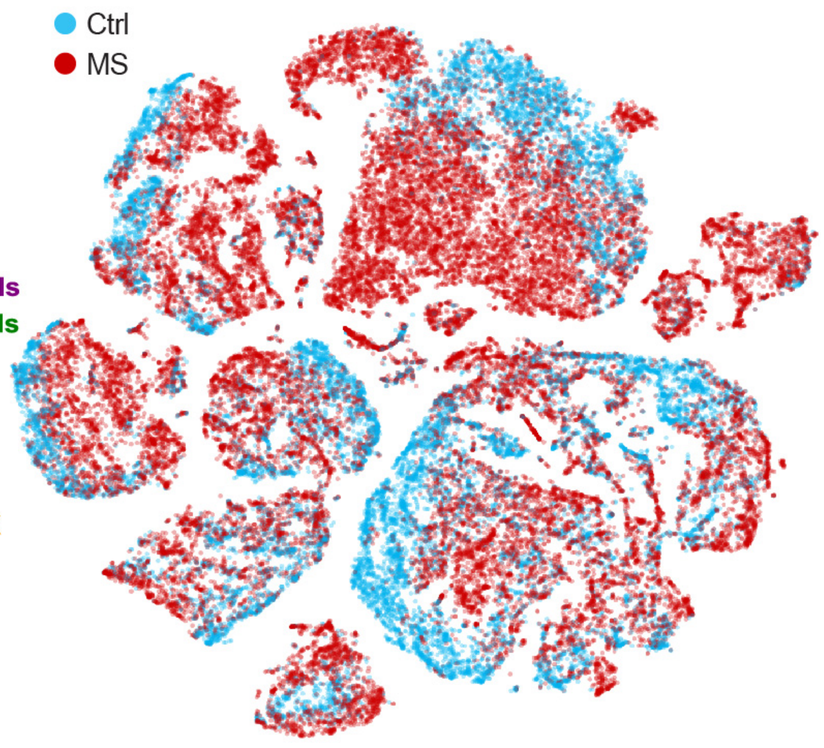

d

Cell-type specific marker gene expression

All neurons — *SYT1*

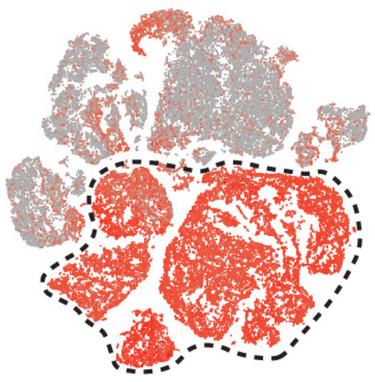

Excitatory neurons — *SLC17A7*

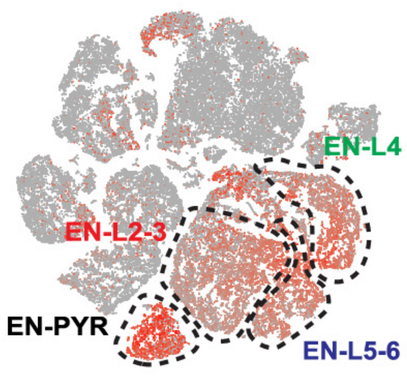

Inhibitory neurons — *GAD2*

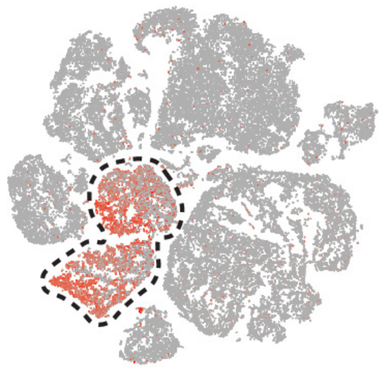

Astrocytes — *AQP4*

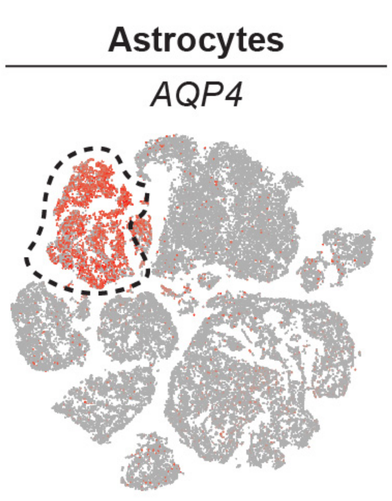

Oligodendrocytes — *PLP1*

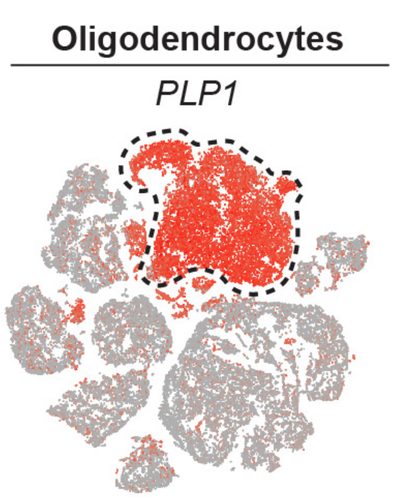

Microglia — *P2RY12*

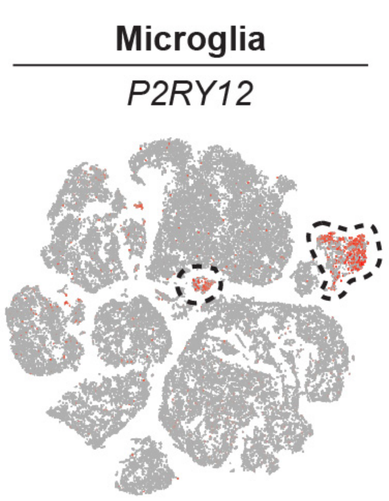

e

Normalized cell numbers per cell cluster

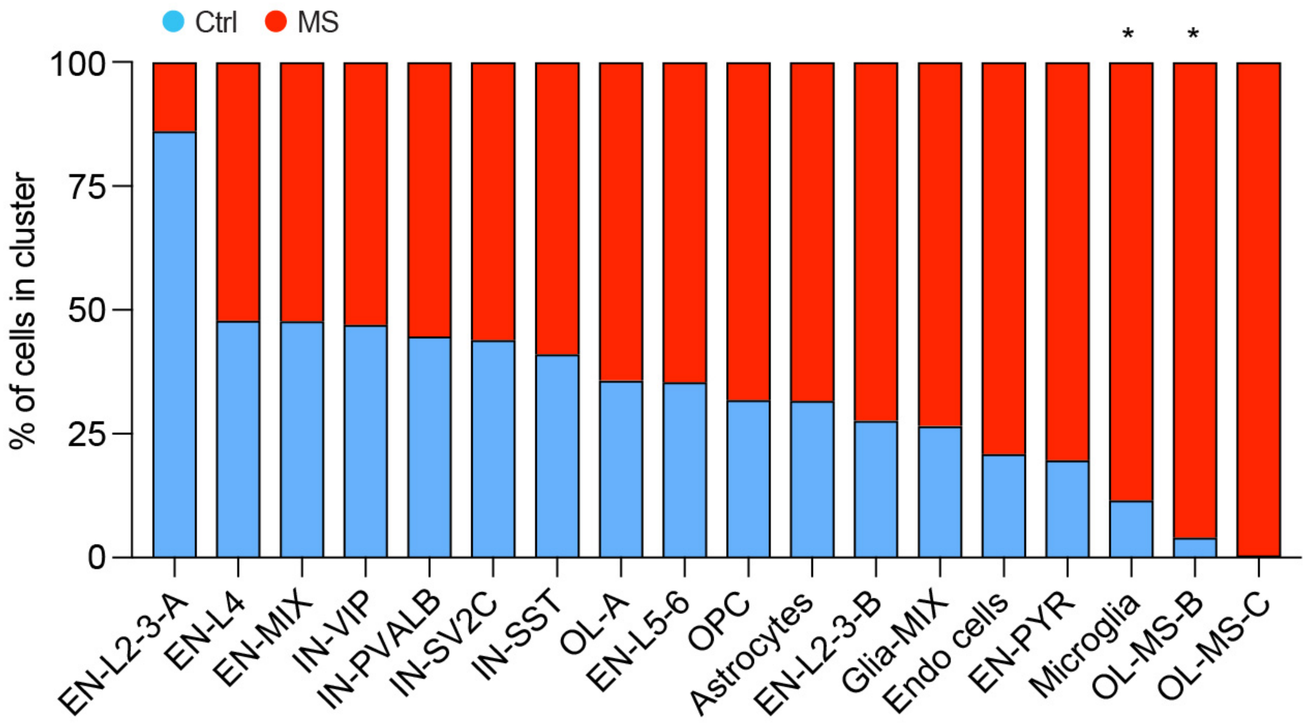

f

Cell-type specific drop out of excitatory L2-3 neurons

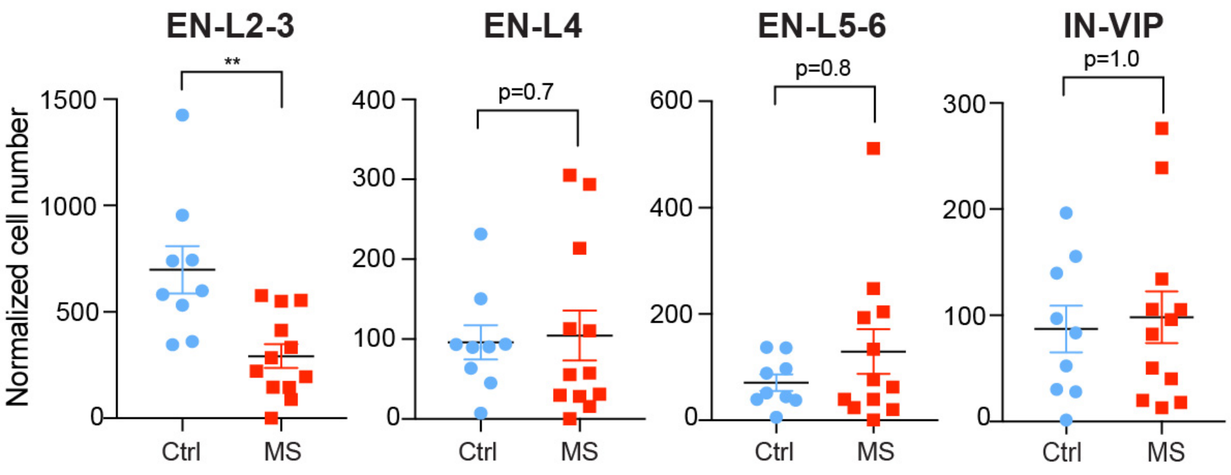

g

Cell-type specific differential gene expression analysis

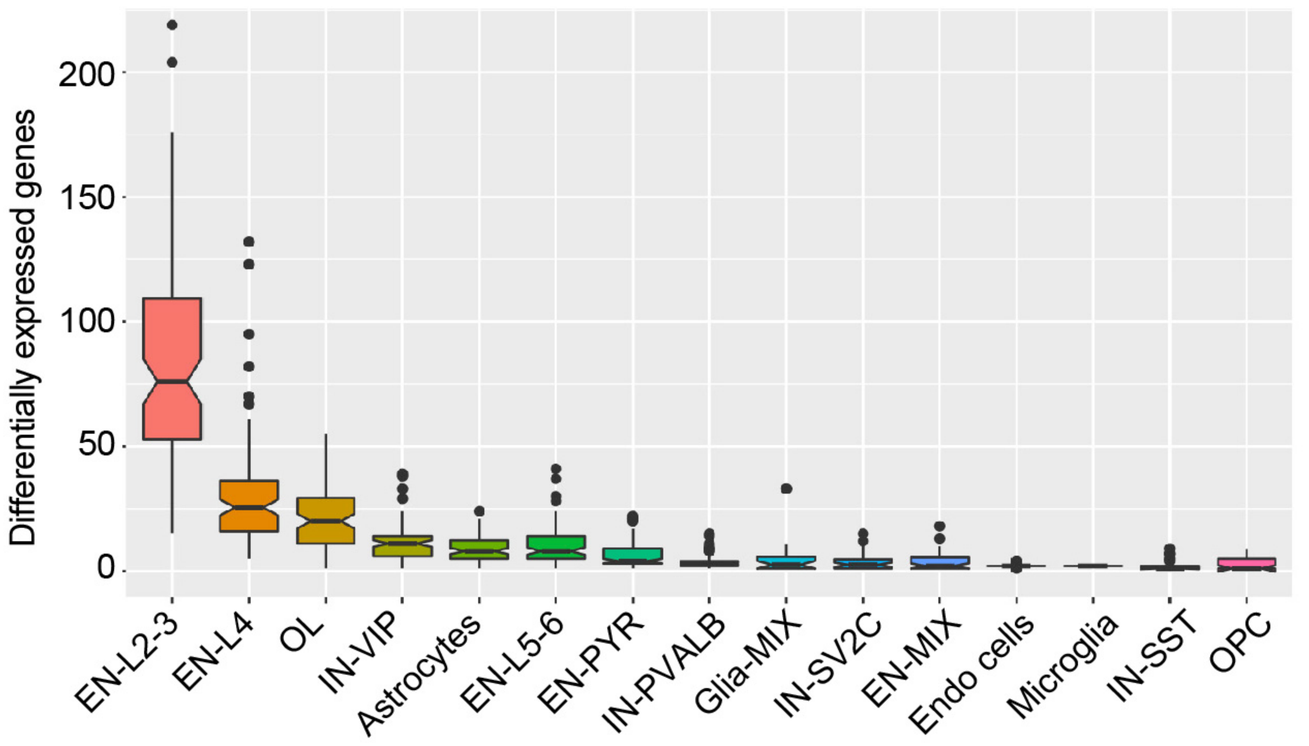

a

EN-L2-3 (upper layer excitatory neurons)

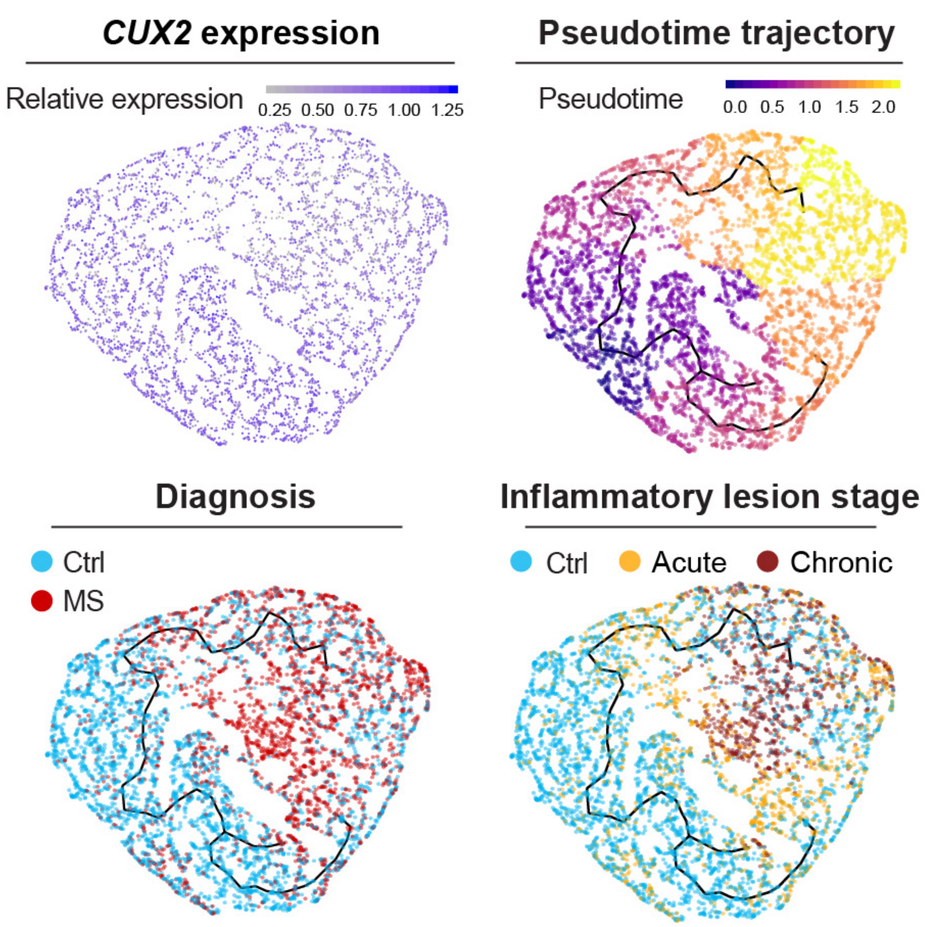

b

EN-L2-3 pseudotime to lesion stage and demyelination

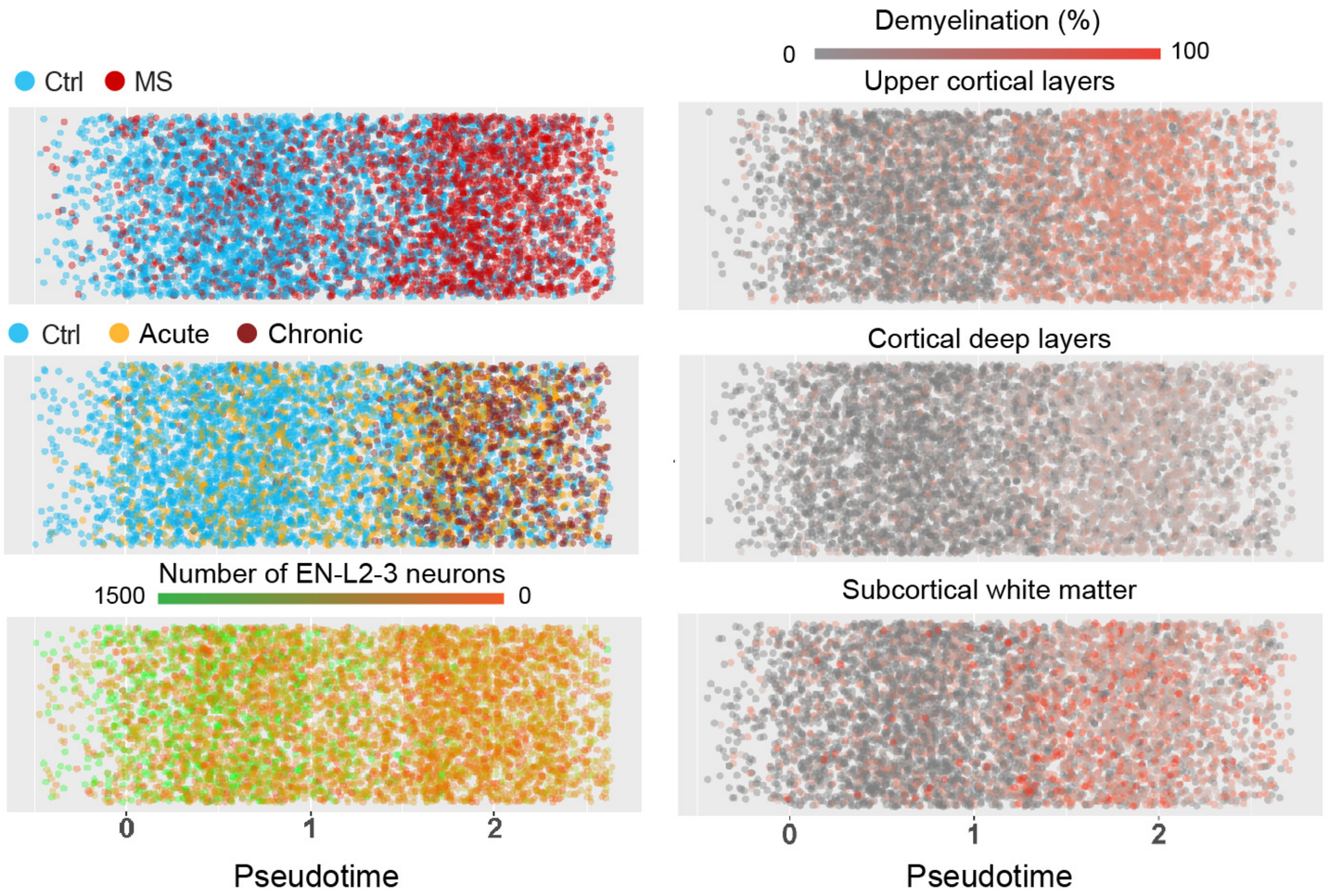

c

Pseudotime density vs. lesion stage

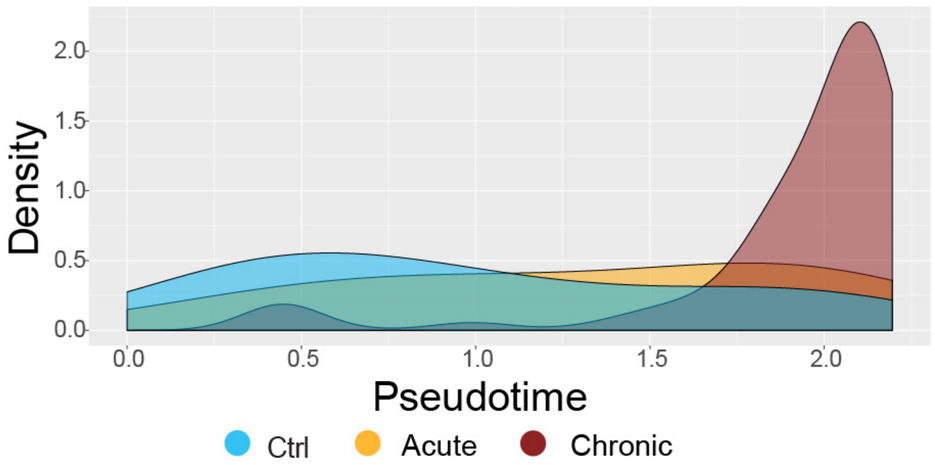

d

GO terms enriched for EN-L2-3 pseudotime-dependent genes

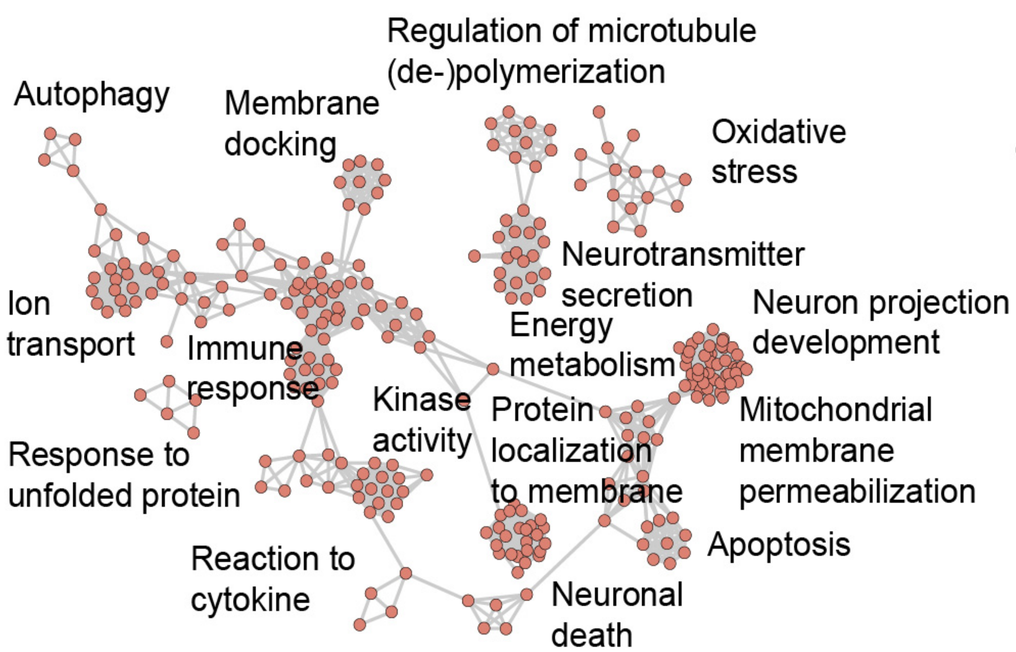

e

Pseudotime-dependent upregulated genes

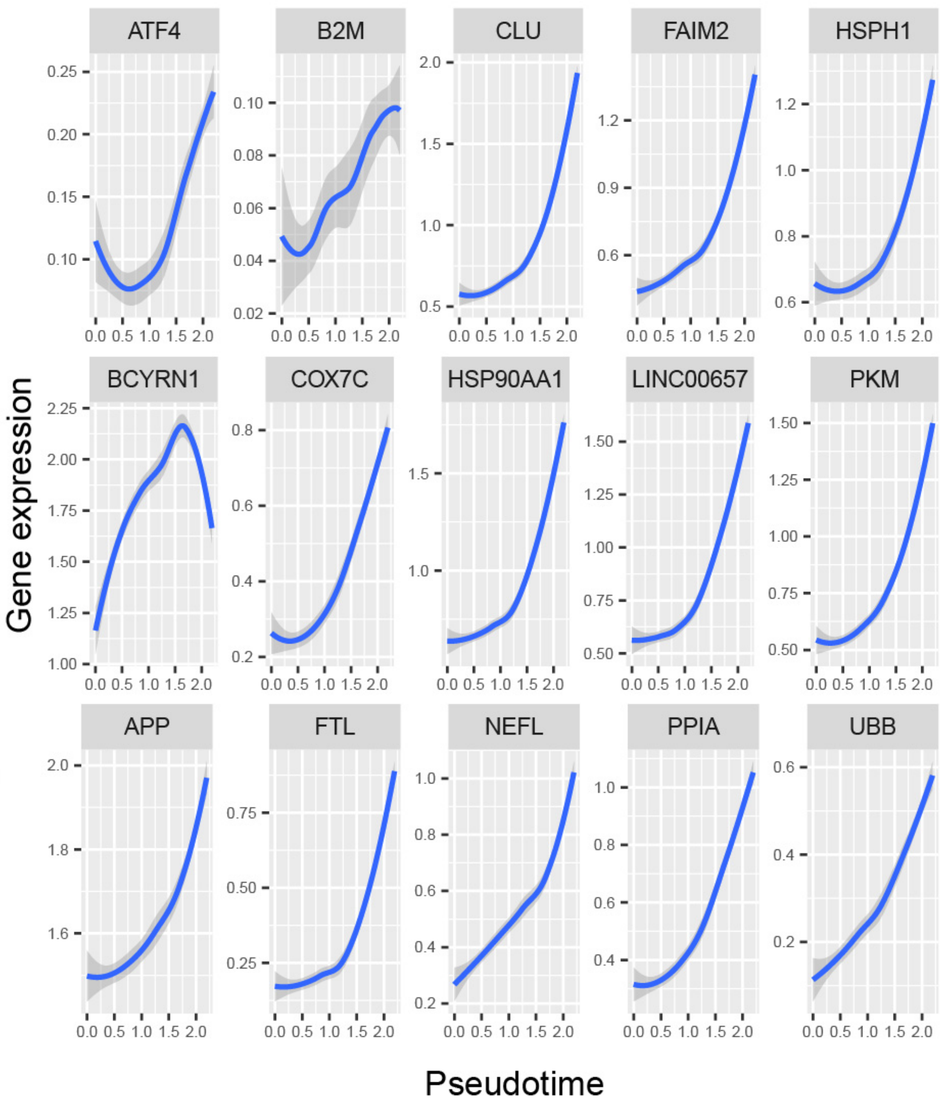

f

Pseudotime-dependent downregulated genes

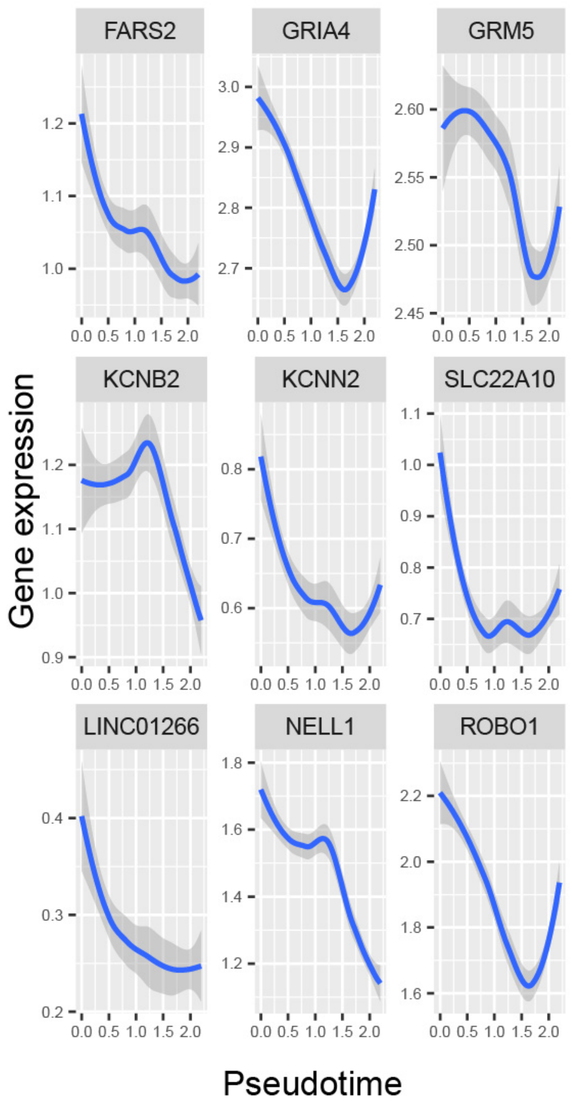

a

Spatial transcriptomic cortical MS pathology and neuron subtype diversity

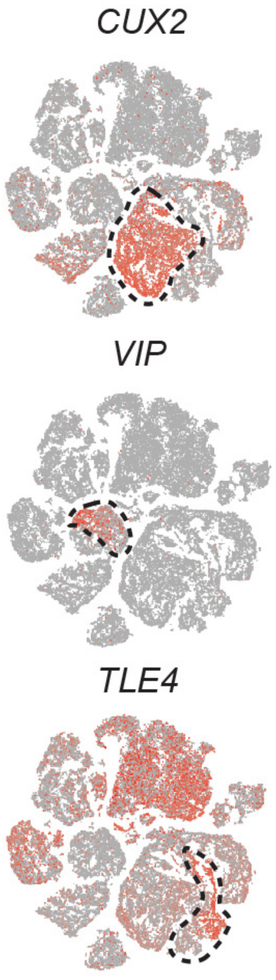

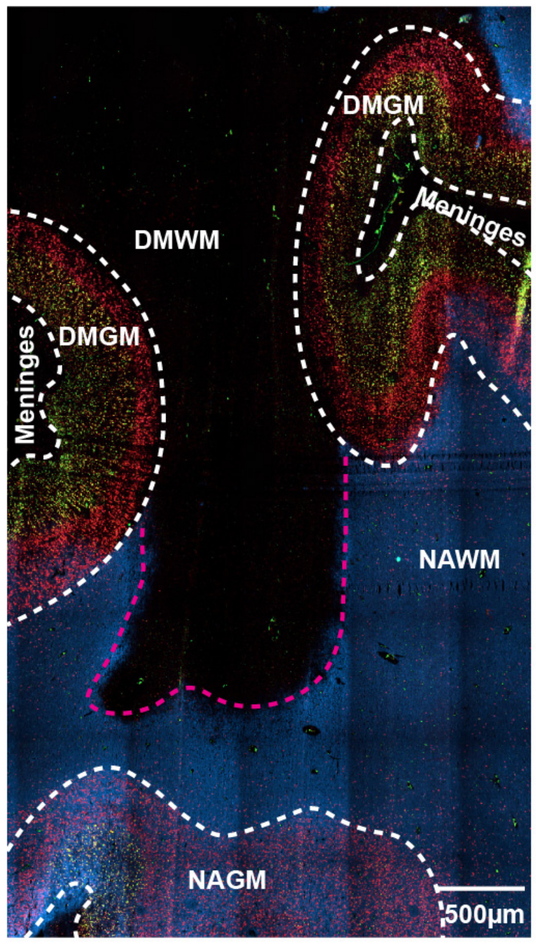

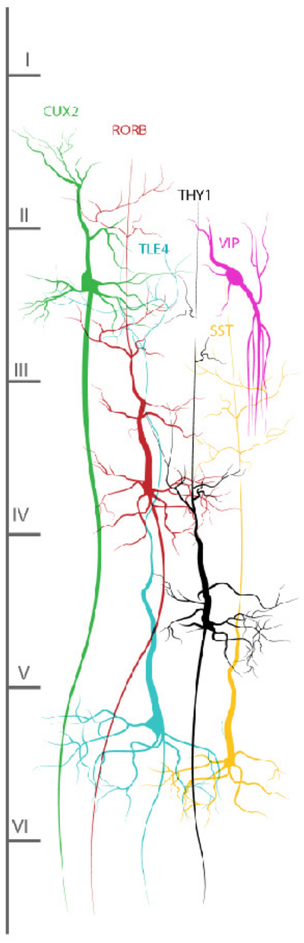

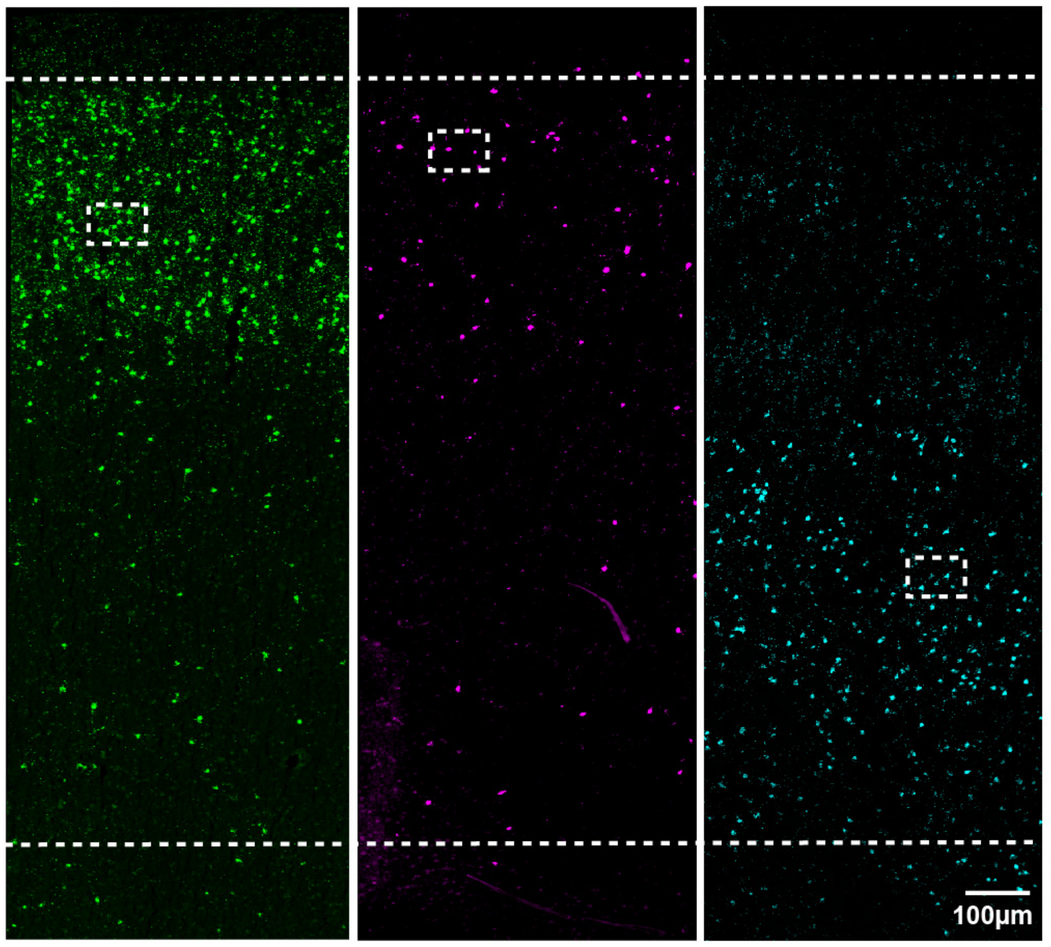

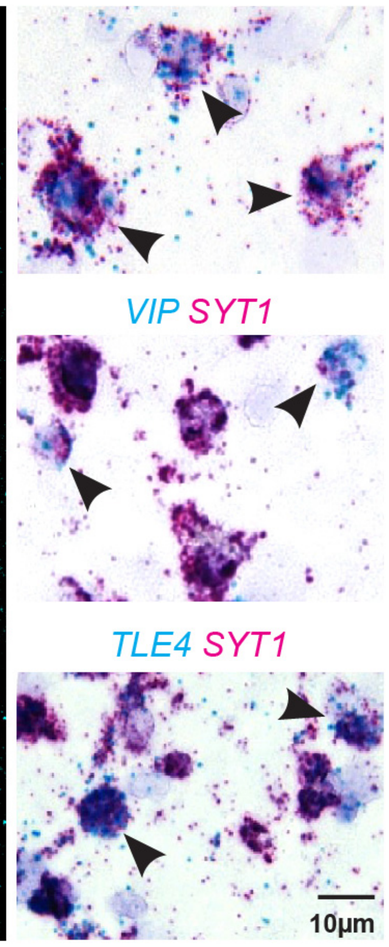

b

Drop-out of upper layer excitatory but not inhibitory neurons in cortical MS lesions

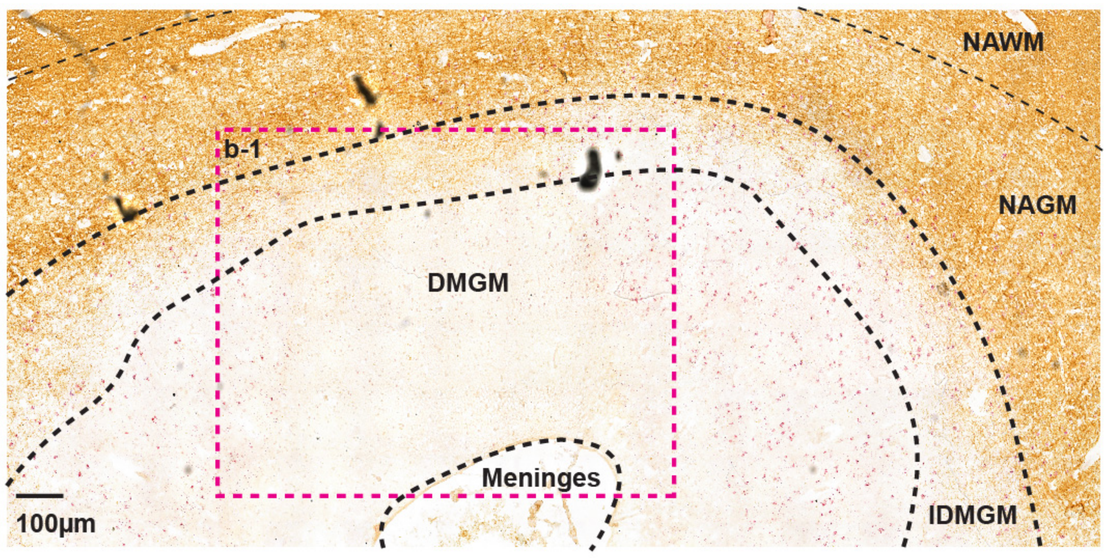

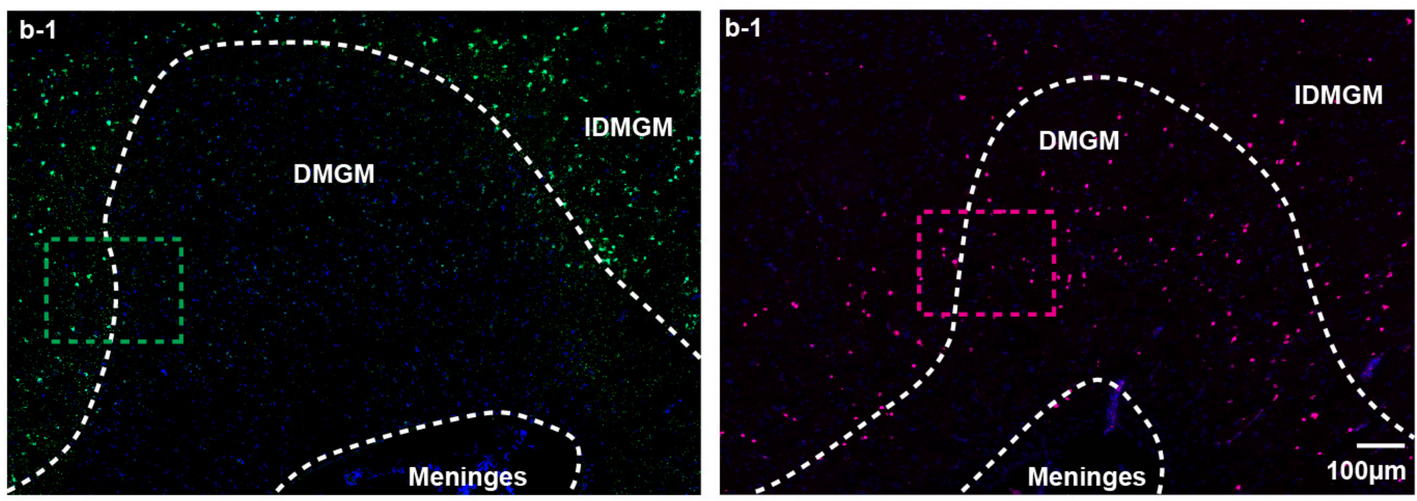

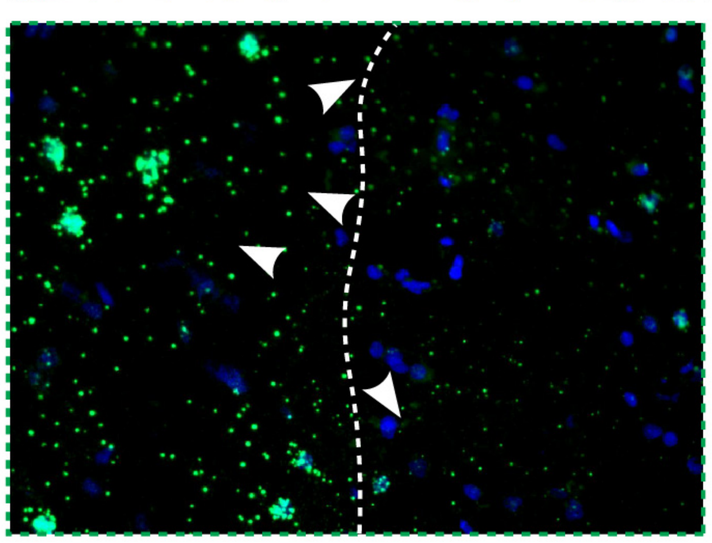

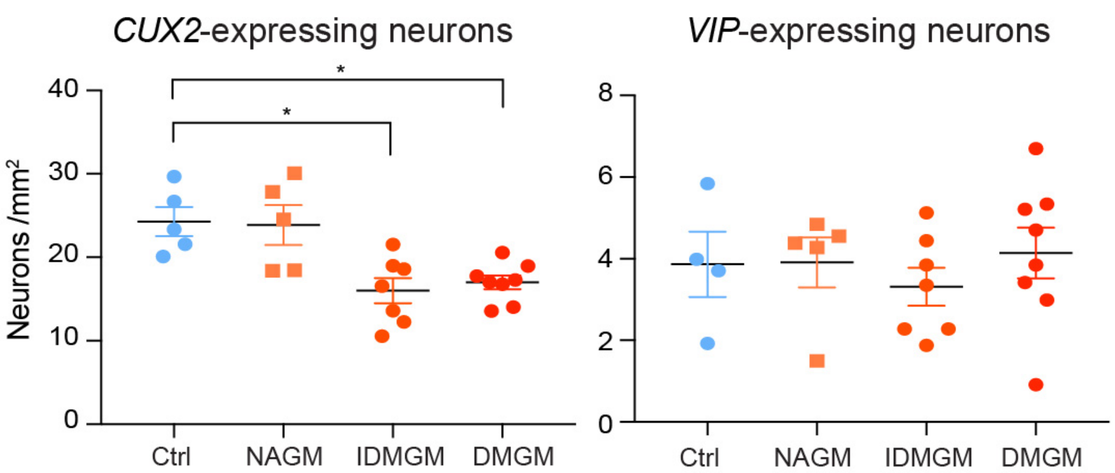

c

Upregulation of neuronal *PPIA* and *LINC00657 (NORAD)* in cortical MS lesions

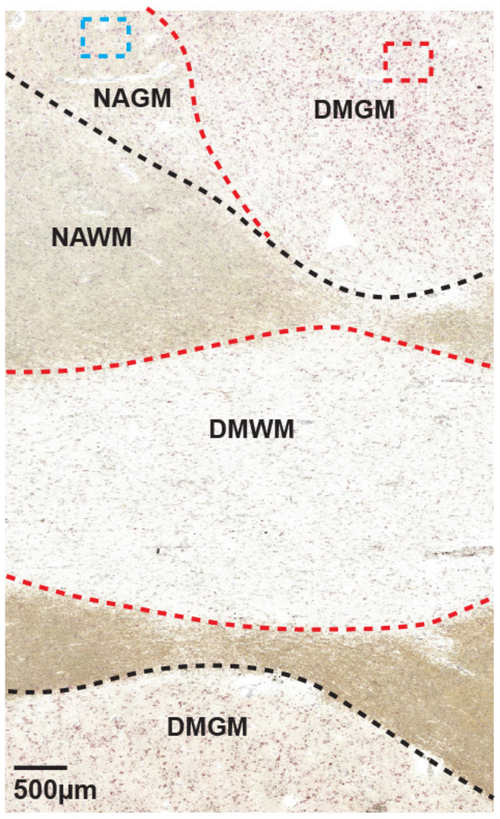

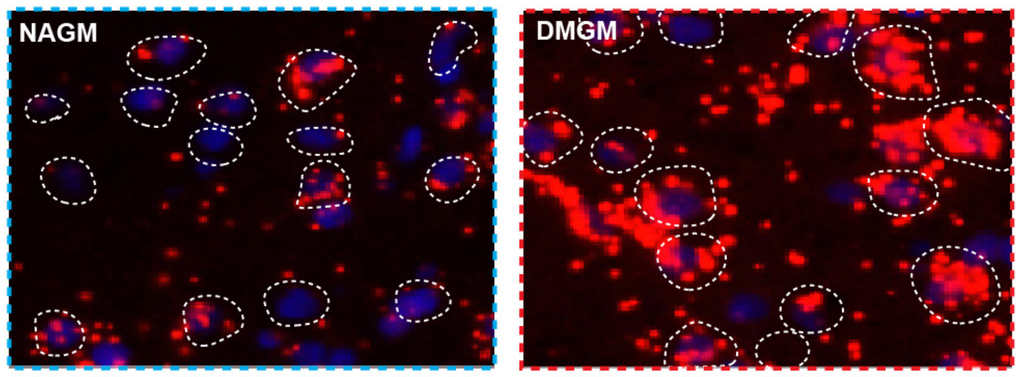

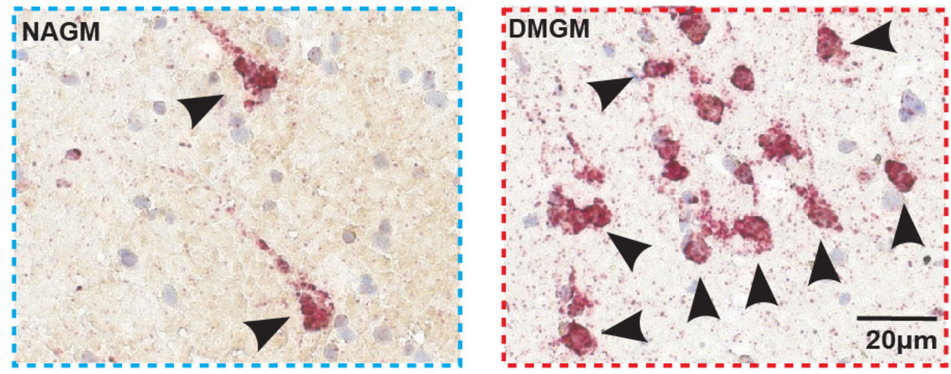

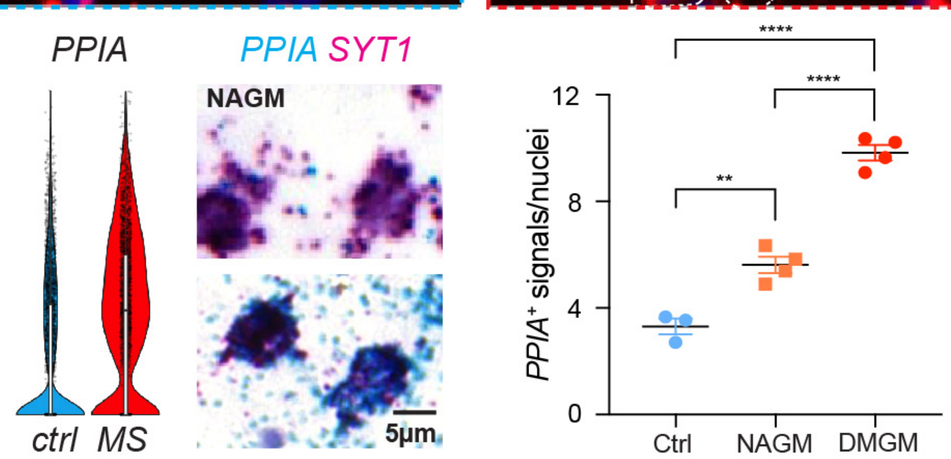

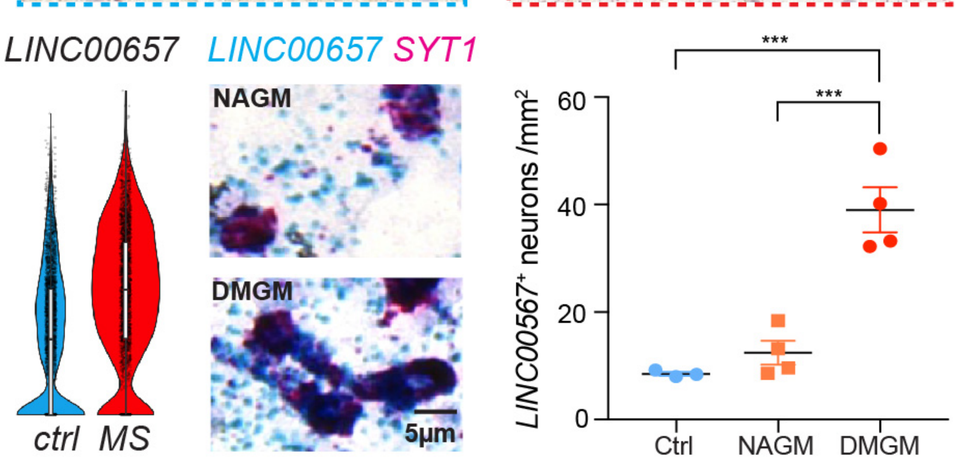

a

Differential astrocyte reactivity between cortical and subcortical MS lesions

SLC1A2 GPC5

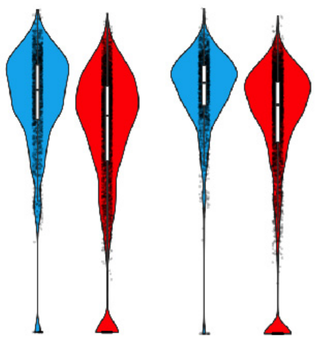

GFAP CD44

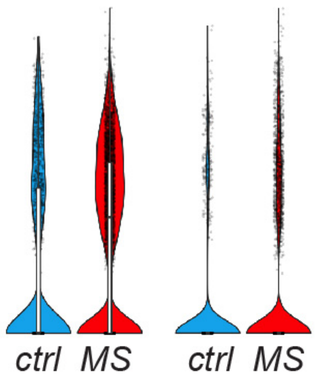

SLC1A2 RFX4 CD44 MOG

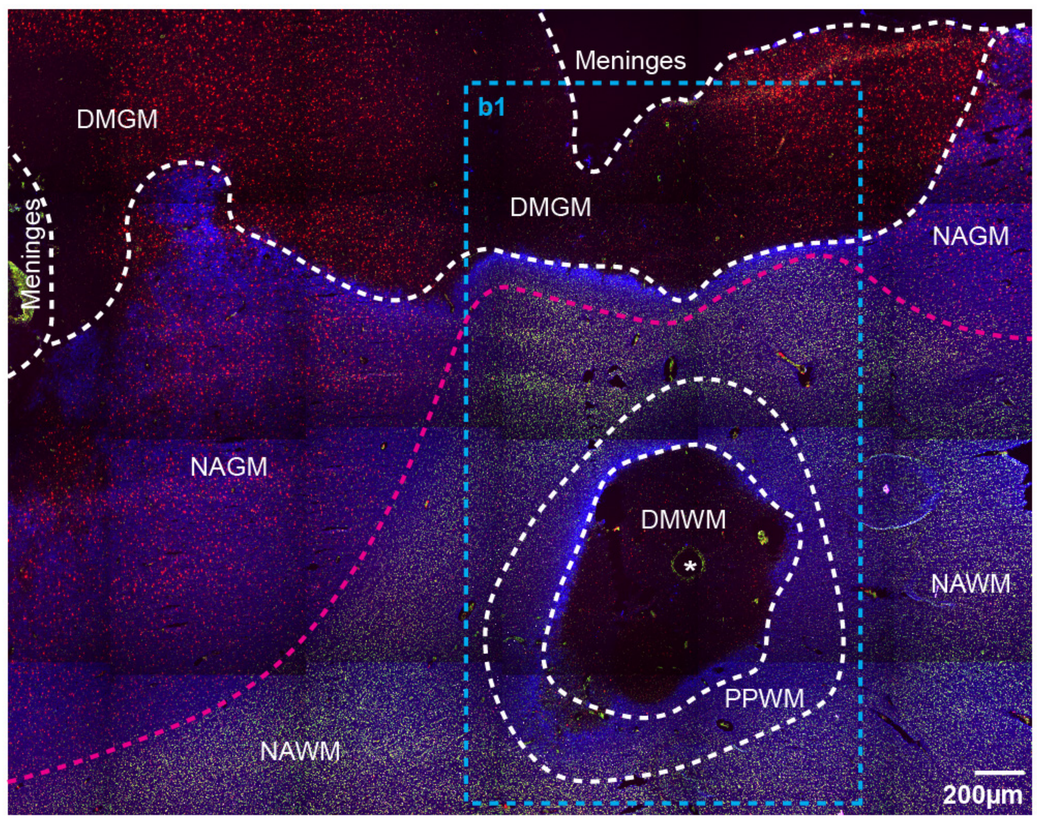

SLC1A2 RFX4 CD44 DAPI

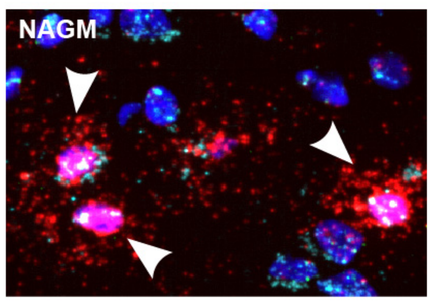

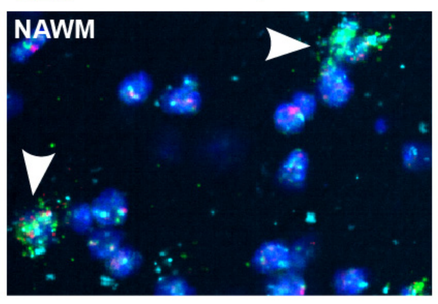

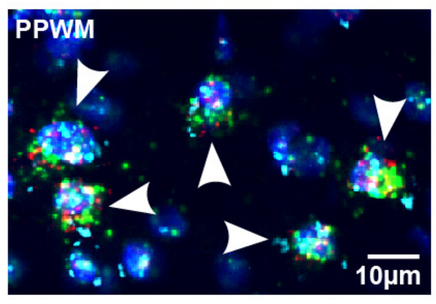

CD44 RFX4

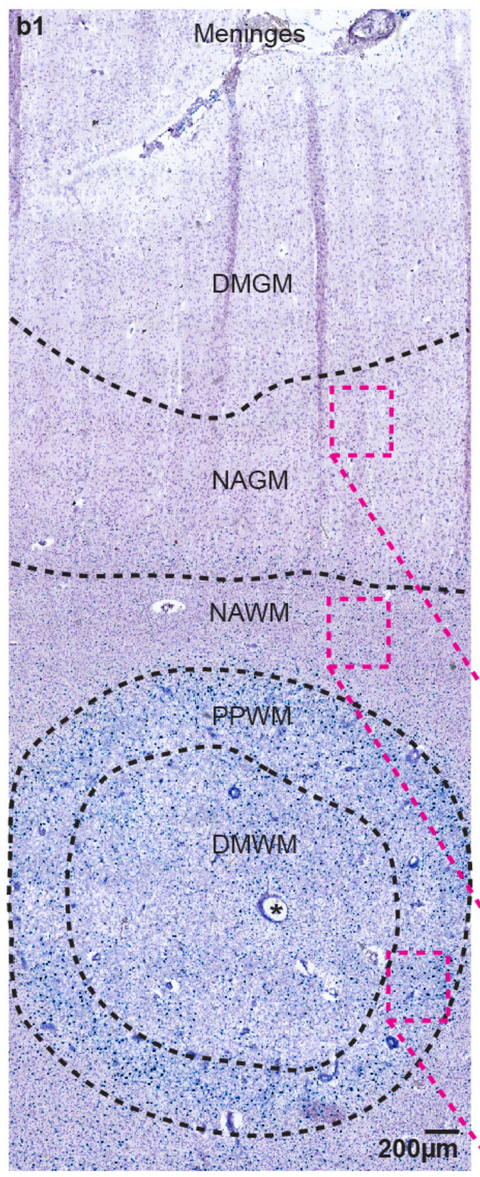

CD44 RFX4

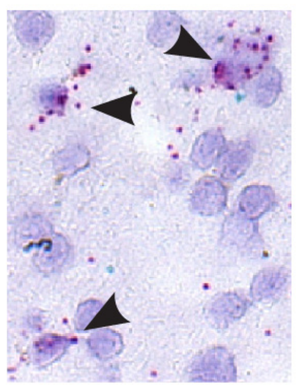

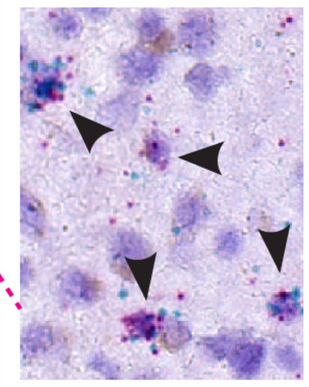

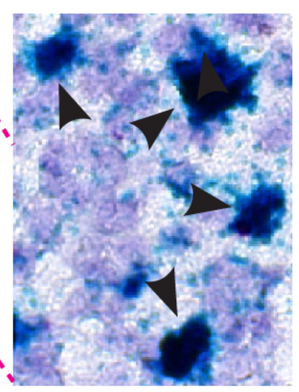

GPC5 RFX4

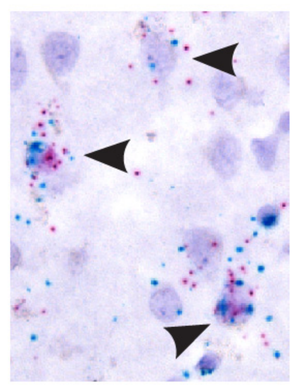

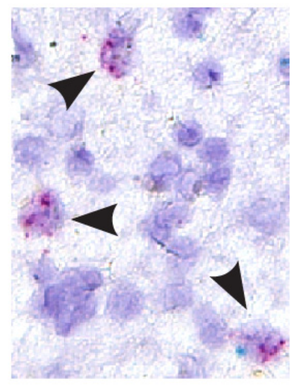

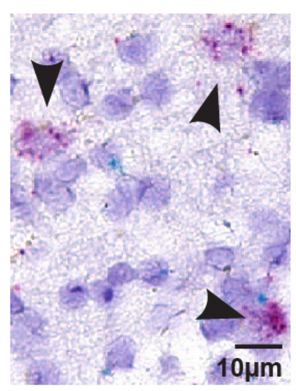

b

Differential gene expression in reactive astrocytes at subcortical lesion rims

Glutamate/K⁺

GLUL KCNJ10

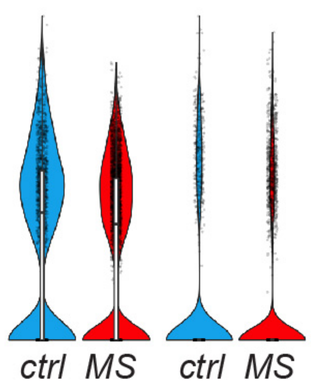

Reactive astrocyte transcription factors and lncRNA

BCL6

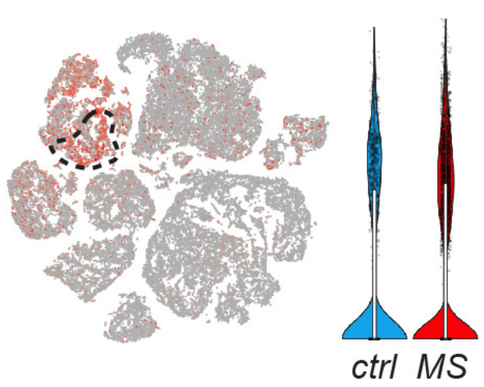

CD44 BCL6

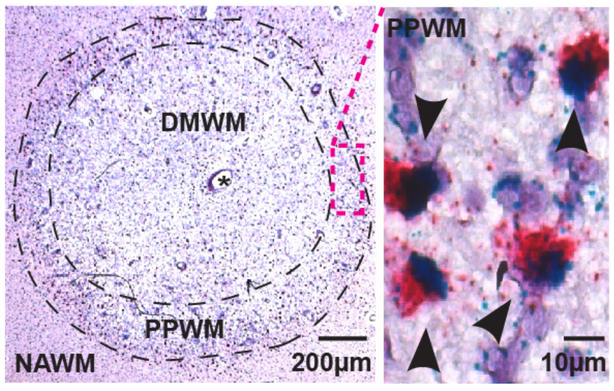

FOS FOS GFAP DAPI

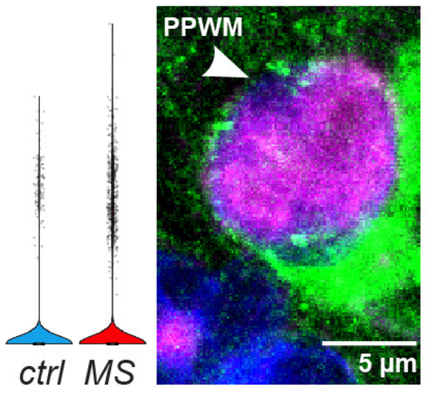

LINC01088 CD44 LINC01088

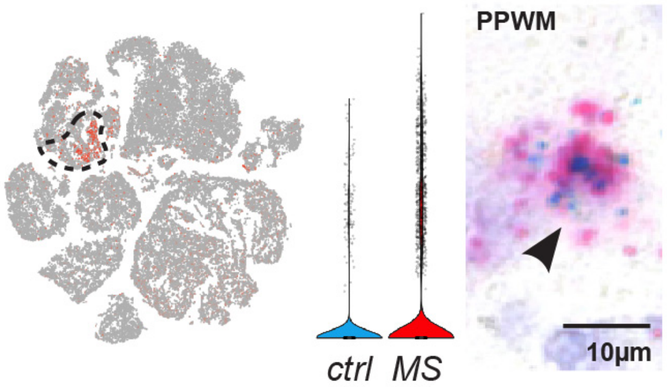

c

Dysregulated marker genes in MS OLs

HSP90AA1 FAIM2 LINC00657 ATF4 UBB

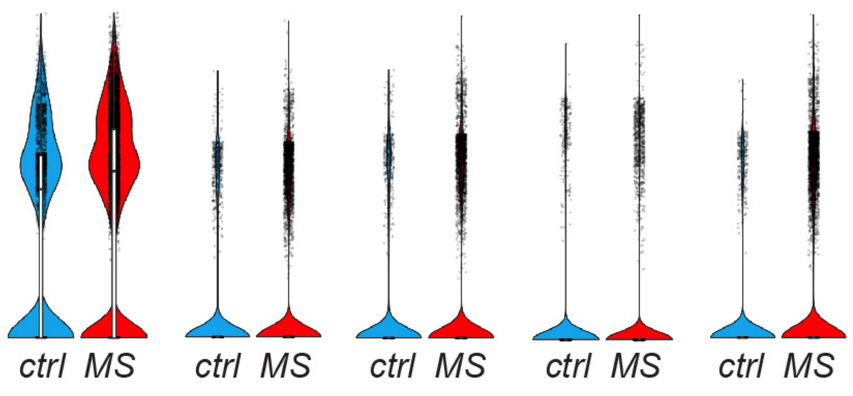

BCAS1 SGMS1 KCNJ10 SEMA6A GLDN

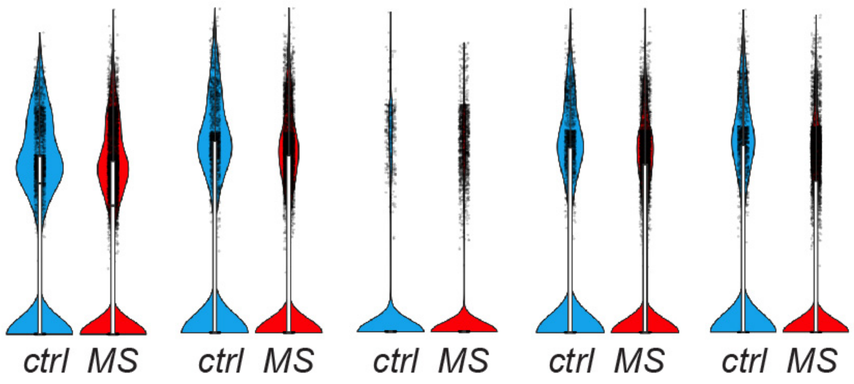

d

Ferritin and MHC-I transcripts upregulated in OLs at subcortical lesion rims

FTL PLP1 FTL

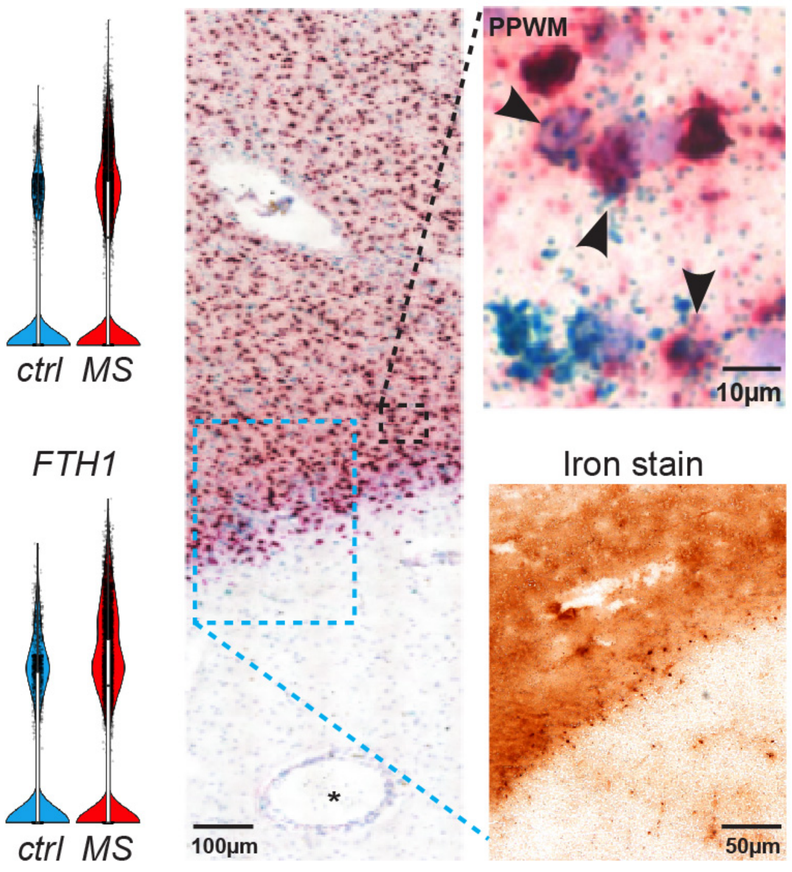

FTH1 Iron stain

B2M PLP1 B2M

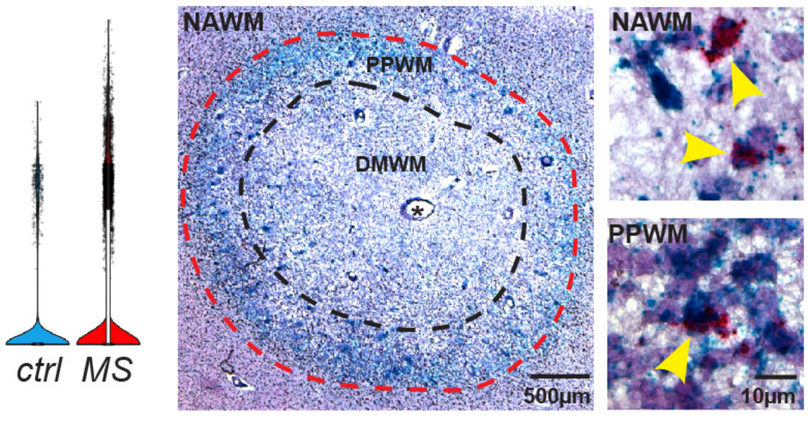

HLA-C PLP1 B2M DAPI

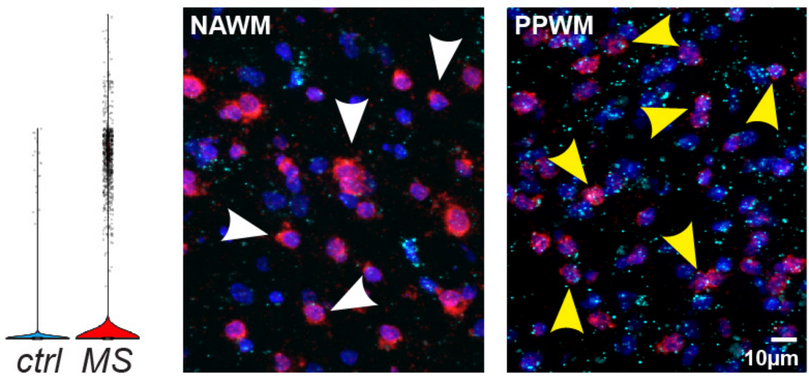

a

Microglia activation patterns in MS lesions

Myelin phagocytosis and breakdown

PLP1 *MBP* *ASAH1* *ACSL1* *DPYD*

Microglia activation markers

CD68 *CD74* *FTL* *APOE* *SPP1*

Macrophage marker *MSR1*

Neuron maintenance

SYNDIG1 *KCNQ3*

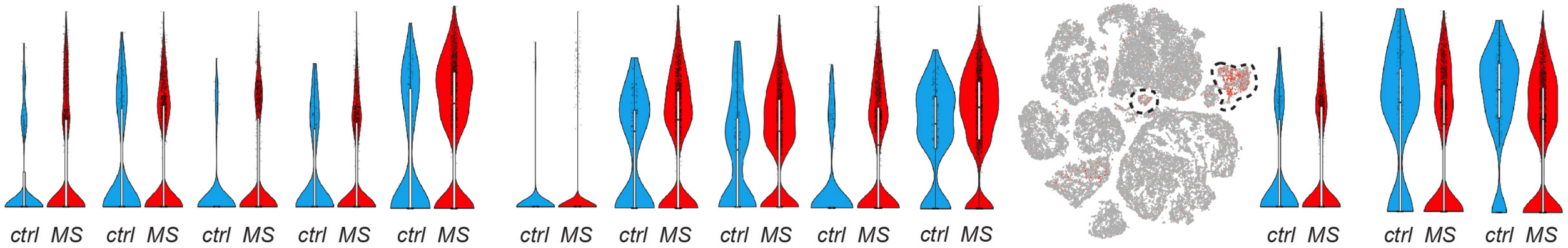

b

Microglia spatial transcriptomic signatures at chronic active MS lesion rims

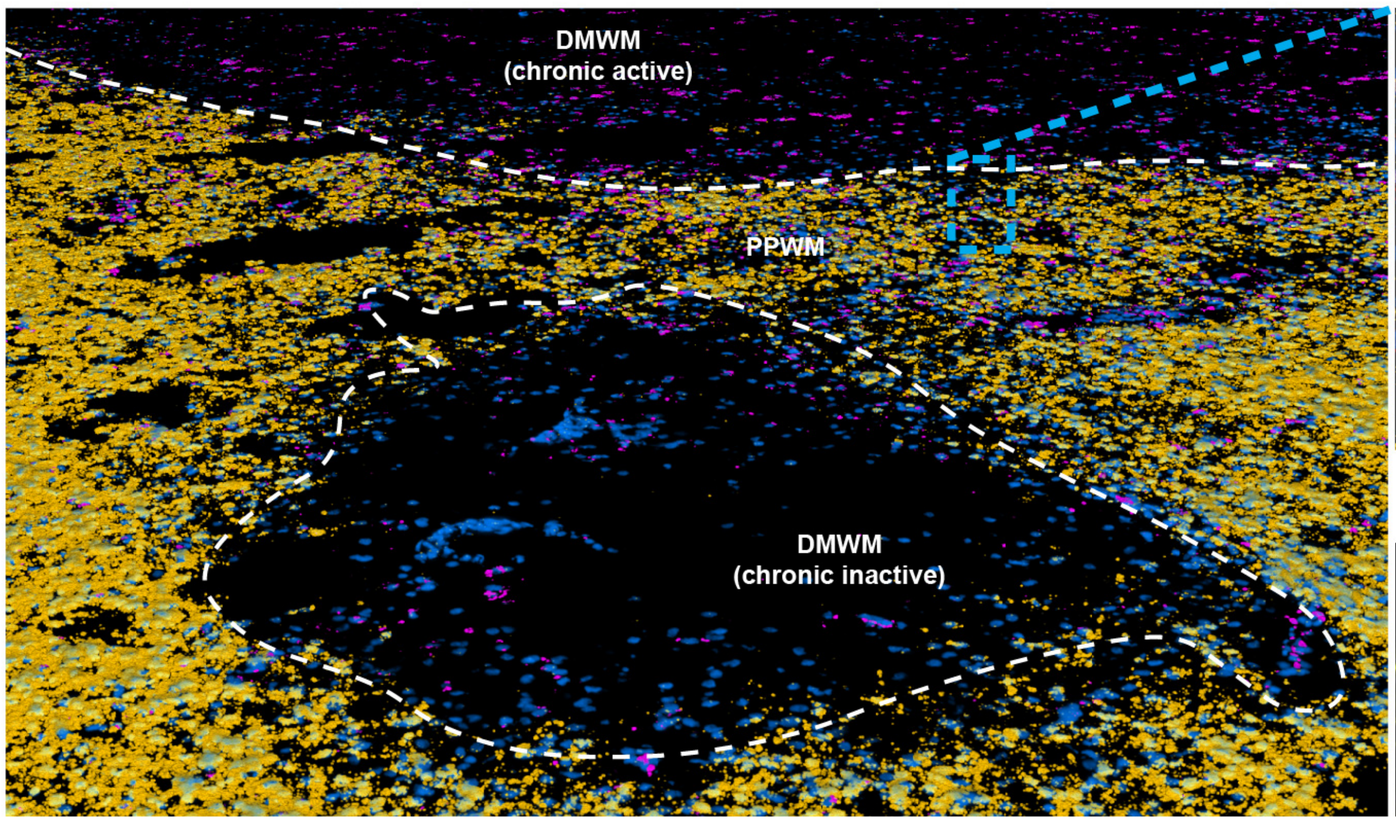

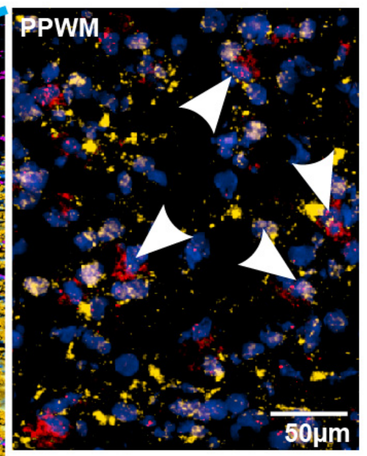

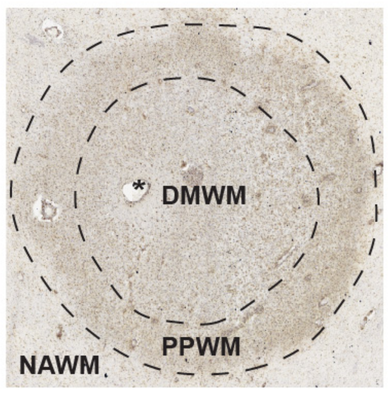

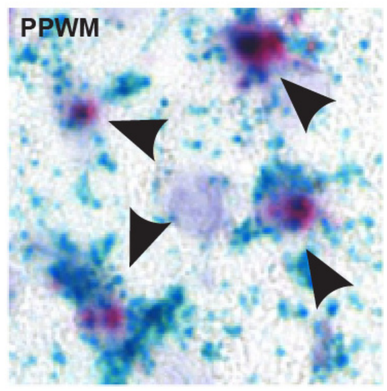

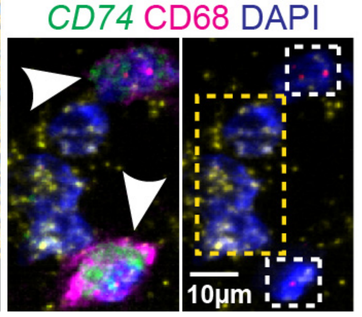

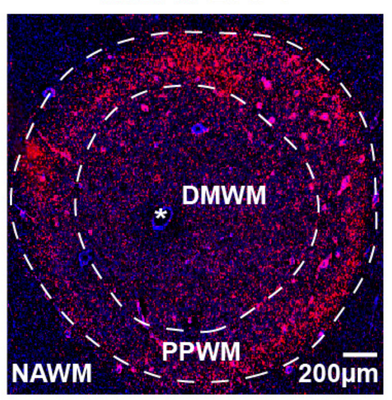

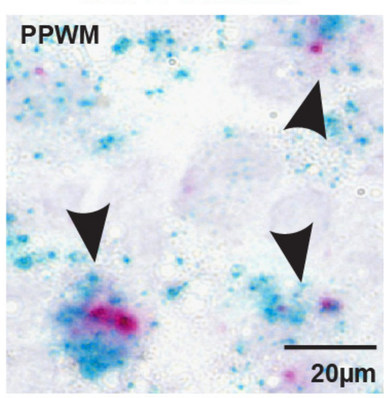

c

Human and mouse myelin-microglia phagocytosis assays

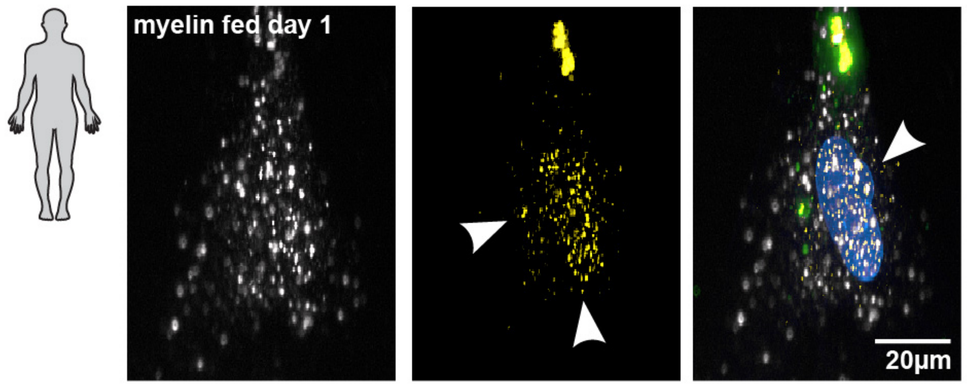

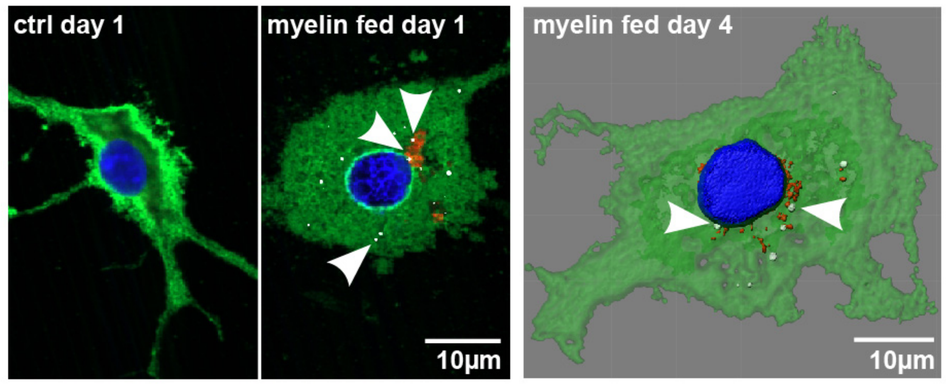

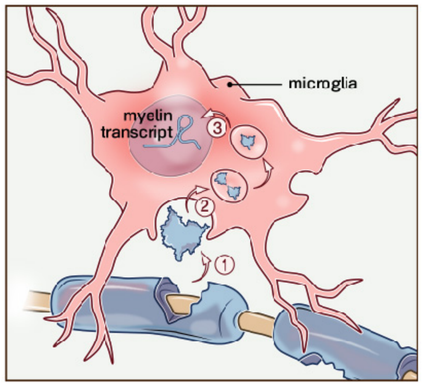

Quantification of ingested myelin RNA in microglia

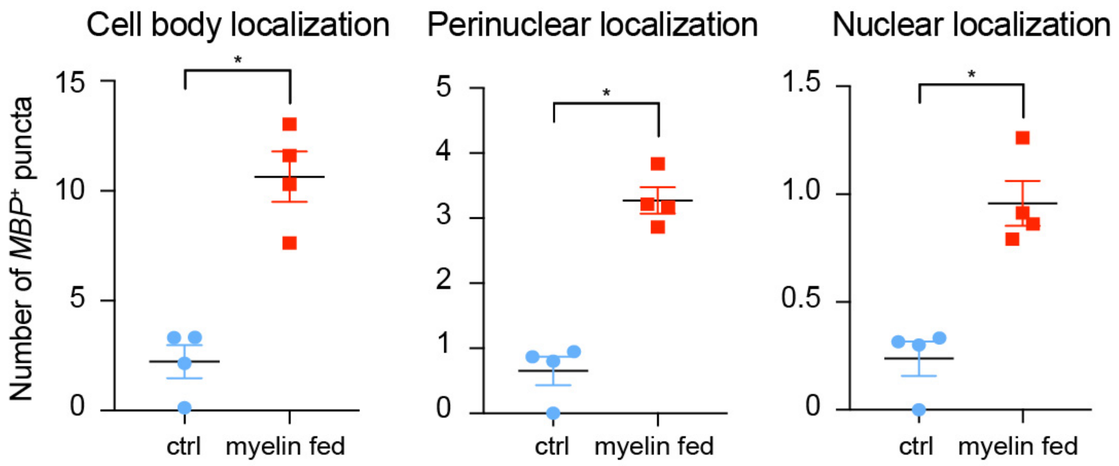

Differential gene expression in phagocytosing microglia